Asian Journal of Chemistry; Vol. 37, No. 10 (2025), 2431-2448
ASIAN JOURNAL OF CHEMISTRY
https://doi.org/10.14233/ajchem.2025.34365

Structural, Spectroscopic, Electronic, Topological and Biological Analysis of Two Phytochemical Compounds as Anti-inflammatory Agents

B. AYSHA RIFANA[1], A. ANURADHA[2] and JOHANAN CHRISTIAN PRASANA[1,*]

[1]Department of Physics, Madras Christian College (Affiliated to University of Madras), East Tambaram, Chennai-600059, India
[2]PG & Research Department of Physics, Queen Mary's College (Affiliated to University of Madras), Chennai-600004, India

*Corresponding author: E-mail: reachjcp@gmail.com

Received: 29 June 2025 *Accepted*: 9 September 2025 *Published online*: 30 September 2025 AJC-22127

4-Hydroxy-3,5-dimethoxybenzoic acid (4HDA) and zingerone are the two phytochemical compounds with significant therapeutic potential. In this work, the structural, electronic and pharmaceutical properties of both compounds were investigated using computational methods. Density Functional Theory (DFT) was employed to investigate the atomic configurations and electronic properties of the target compounds. Spectroscopic analyses, including FT-IR, FT-Raman, and UV-Visible spectroscopy, were conducted to validate the structural characteristics. Frontier Molecular Orbital (FMO) analysis provided global reactivity descriptors to evaluate molecular stability and reactivity. Transition density matrix (TDM) heat maps were used to examine electronic excitation pathways, while molecular electrostatic potential (MEP) mapping identified electrophilic and nucleophilic regions. Topological analysis further elucidated surface characteristics, and drug-likeness assessments confirmed that both compounds fall within the optimal range for pharmaceutical applicability. Blood-brain barrier, gastrointestinal absorption and metabolic stability were also studied. Half-maximal inhibitory concentration of 4HDA and zingerone on the L929 cell line was obtained through MTT assay. Molecular docking studies revealed strong binding affinities of 4HDA and zingerone with protein 2az5 (TNF alpha protein) and 2bxk (macrophage inflammatory protein 2), showing better interactions compared to the commercially available drug (mesalamine). These findings suggest that 4HDA and zingerone can be potential candidates for inflammatory bowel disease.

Keywords: DFT, Frontier molecular orbital, Molecular electrostatic potential, Drug likeness, Cytotoxicity, Molecular docking.

INTRODUCTION

In recent years, there has been growing scientific interest in the use of phytochemicals for the management and treatment of various medical conditions. In present study, two phytochemical compounds, hydroxy-3,5-dimethoxybenzoic acid (4HDA) and zingerone were chosen to study there structural and biological properties. 4HDA is a common phenolic component discovered in many vegetables (radish), fruits (acai berry, olives, grapes, pumpkin) [1], spices, cereals (barley, oats, wheat, corn), cane sugar and honey [2-4]. It is one of the primary phenol compounds found in sugarcane syrup, giving as much as 10 µg/g dry extracts [5,6]. These sugarcane extracts exhibit substantial antioxidant effects, enhanced regulation of metabolic function and inflammation, as well as antibacterial and anticancer properties [4,7]. It has a broad spectrum of pharmaceutical potential for reducing the risk of cardiovascular disease, cancer and brain ischemia. It possesses an excellent free radical scavenger and reduces oxidative stress indicators [4,8]. The presence of methoxy groups on the benzene ring at sites 3 and 5 essentially gives 4HDA its medicinal prop-erties [8]. Whereas, zingerone, a compound derived from ginger (*Zingiber officinale*), possesses a *p*-substituted hydroxyl group on its benzene ring, which contributes to its notable antioxidant activity. Zingerone, featuring a ketone group linked to a three-carbon aliphatic chain, exhibits significant biological activity [9]. Its water solubility and structural stability enhance its efficacy as a bioactive compound in diverse applications [10]. It functions as a potent antimicrobial and antioxidant agent, effectively scavenging free radicals and reducing oxidative stress [9,11]. Moreover, zingerone demonstrates strong anti-inflammatory properties by inhibiting inflammatory mediators [12] and offers multiple health benefits, including digestive support, cardioprotection, blood sugar regulation, neuroprotection and potential prevention of Alzheimer's disease [9,13].

Chronic diseases collectively referred to as inflammatory bowel disease (IBD) result in continued inflammation of the gastrointestinal system, significantly affecting digestive health. There are two main types of IBD, for example, ulcerative intestinal colitis, which only affects the rectum and bowel and Crohn's disease, which can affect any region of the digestive tract [14]. Although the exact cause of IBD remains unclear, it is widely believed to result from a combination of environmental triggers, genetic predisposition and an abnormal immune response. Decreased weight, exhaustion, constipation, bleeding from the rectal and abdominal discomfort are the typical symptoms [15]. The immune system accidentally targets the gastrointestinal tract, resulting in persistent inflammation and tissue injury. Several factors, such as genetics, smoking and certain medications, may increase the risk of developing IBD [16]. Diagnosis typically involves endoscopic procedures, imaging techniques and laboratory tests to identify inflammation and filter out other illness. Treatment options for IBD include anti-inflammatory medications, immunosuppressive agents, biological therapies, and in severe cases, surgical removal of the affected intestinal segments [17]. Lifestyle modifications, including dietary changes, stress management and physical activity, are essential for controlling symptoms and enhancing life quality. In order to enhance long-term patient outcomes, researchers are making attempts to comprehend the causes of IBD and create enhanced treatments [18].

Since both compounds, 4HDA and zingerone have strong anti-inflammatory activity, an effort is made to utilize 4HDA and zingerone in inflammatory bowel disease (IBD), an inflammatory disease through molecular docking analysis. Extensive computational studies on the compounds 4HDA and zingerone have not been documented in the literature. Hence, an attempt is made to study the optimized structure, vibrational spectroscopy, electron density analysis, reactive sites and pharmaceutical activities of 4HDA and zingerone.

METHODOLOGY

Computational details: Theoretical calculations based on Density Functional Theory (DFT) were performed using the Gaussian 16W software package [19,20]. The B3LYP functional with the 6-311++G(d,p) basis set was employed, as this level of theory offers reliable predictions for molecular geometries, electronic properties, and reactive sites [21]. The molecular structures of 4HDA and zingerone were optimized, and their bond parameters were subsequently determined. The vibrational wavenumbers, Raman activity, IR intensity and potential energy distribution assignments were acquired from VEDA software [22]. Utilizing GaussSum software [23], UV assignments were obtained. Multiwfn 3.7, Multiwfn 3.8 [24] and VMD [25] were used to address the topological reactive sites. Nucleophilic and electrophilic regions were also examined. The biological analyses such as drug likeness, Ramachandran plot and molecular docking analysis were also investigated using SwissADME [26], Procheck [27] and AutoDock tools-1.5.6 [28].

Experimental details: 4-Hydroxy-3,5-dimethoxybenzoic acid (4HDA) and zingerone, with a concentration of 97% and 98%, was sourced from TCI Chemical Company, India and used directly without further purification. FT-IR spectrum (4000-500 cm^{-1}) was recorded at the Sophisticated Analytical Instrumentation Facility (SAIF) at IIT-Madras, India using a Perkin-Elmer FTIR spectrophotometer and FT-Raman spectrum (4000-100 cm^{-1}) with a Bruker RFS 27 spectrophotometer, respectively. Cytotoxicity evaluations, including MTT assays to determine the toxicity and IC_{50} values of 4HDA and zingerone, were conducted using the L929 cell line at the Pondicherry Centre for Biological Science and Educational Trust, India.

RESULTS AND DISCUSSION

Geometrical analysis: Density functional theory (DFT) was utilized to determine the molecular bond lengths and bond angles accurately, providing information into the geometry and electronic structure of molecules [29]. Fig. 1 illustrates the optimized geometric structures of 4HDA and zingerone, while Table-1 presents their corresponding bond parameters.

Bond characteristics of 4HDA and zingerone offer critical information regarding its structural properties. Bond length of C2-C21 in 4HDA is 1.480 Å and C1-C2 in zingerone is 1.521 Å, which are the longest bonds in both compounds as they are carbon-carbon single bonds and the atoms electronegativities are relatively equal. Such bonds are non-polar, which increases their flexibility. Meanwhile the lowest bond length of O10-H11 in 4HDA is 0.968 Å, whereas in zingerone the

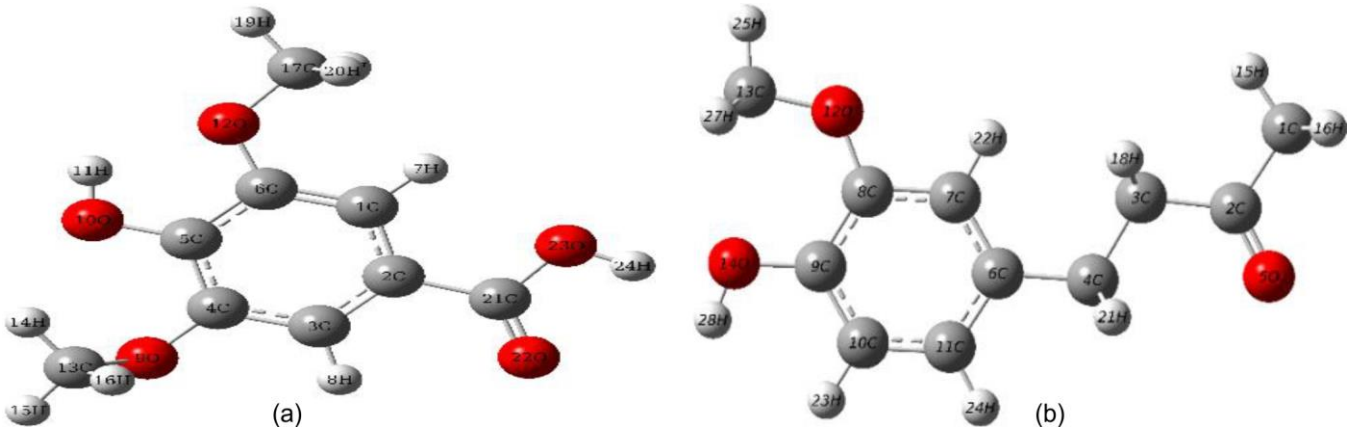

Fig. 1. Geometrical structure of (a) 4HDA and (b) zingerone

TABLE-1
OPTIMIZED GEOMETRICAL PARAMETERS OF
4HDA AND ZINGERONE USING B3LYP/6-311++G(d,p)

4HDA		Zingerone	
Bond length (Å)		Bond length (Å)	
C1-C2	1.404	C1-C2	1.521
C1-C6	1.385	C1-H15	1.091
C1-H7	1.080	C1-H16	1.093
C2-C3	1.395	C1-H17	1.093
C2- C21	1.480	C2-C3	1.520
C3-C4	1.392	C2-O5	1.212
C3-H8	1.082	C3-C4	1.524
C4-C5	1.401	C3-H18	1.098
C4-O9	1.369	C3-H19	1.098
C5-C6	1.408	C4-C6	1.518
C5-O10	1.357	C4-H20	1.095
C6-O12	1.372	C4-H21	1.095
O9-C13	1.435	C6-C7	1.391
O10-H11	0.968	C6-C11	1.401
O12-C17	1.425	C7-C8	1.403
C13-H14	1.091	C7-H22	1.083
C13-H15	1.089	C8-C9	1.403
C13-H16	1.095	C8-O12	1.366
C17-H18	1.094	C9-C10	1.397
C17-H19	1.088	C9-O14	1.381
C17-H20	1.094	C10-C11	1.387
C21-O22	1.210	C10-H23	1.087
C21-O23	1.363	C11-H24	1.085
O23-H24	0.968	O12-C13	1.431
H11-O12	2.069	C13-H25	1.090
O22-H24	2.270	C13-H26	1.091
Bond angle (º)		C13-H27	1.091
C2-C1-C6	119.0	O14-H28	0.962
C2-C1-H7	119.6	Bond angle (º)	
C1-C2-C3	120.3	C2-C1-H15	113.1
C1-C2- C21	121.5	C2-C1-H16	108.9
C6-C1-H7	121.4	C2-C1-H17	108.9
C1-C6-C5	121.0	C1-C2-O3	116.7
C1-C6-O12	125.9	C1-C2-O5	120.8
C3-C2- C21	118.1	H15-C1-H16	109.3
C2-C3-C4	120.7	H15-C1-H17	109.3
C2-C3-H8	120.1	H16-C1-H17	107.2
C2-C21-O22	125.5	C3-C2-O5	122.5
C2- C21-O23	113.0	C2-C3-C4	113.9
C4-C3-H8	119.2	C2-C3-H18	107.1
C3-C4-C5	119.3	C2-C3-H19	107.1
C3-C4-O9	119.0	C4-C3-H18	111.6
C5-C4-O9	121.6	C4-C3-H19	111.6
C4-C5-C6	119.7	C3-C4-C6	116.2
C4-C5-O10	120.3	C3-C4-H20	108.5
C4-O9-C13	116.6	C3-C4-H21	108.5
C6-C5-O10	120.0	H18-C3-H19	105.0
C5-C6-O12	113.1	C6-C4-H20	109.0
C5-O10-H11	107.6	C6-C4-H21	109.0
C6-O12-C17	118.5	C4-C6-C7	123.5
C6-O12-H11	84.5	C4-C6-C11	119.0
O9-C13-H14	111.4	H20-C4-H21	104.9
O9-C13-H15	105.8	C7-C6-C11	117.6
O9-C13-H16	110.3	C6-C7-C8	123.0
O10-H11-O12	114.8	C6-C7-H22	121.4
O12-C17-H18	111.0	C6-C11-C10	120.3
O12-C17-H19	105.9	C6-C11-H24	120.1
O12-C17-H20	111.0	C8-C7-H22	115.6
C17-O12-H11	156.8	C7-C8-C9	118.5
H14-C13-H15	109.8		
H14-C13-H16	110.0		
H15-C13-H16	109.4		
H18-C17-H19	109.6		
H18-C17-H20	109.7		
H19-C17-H20	109.6		
O22- C21-O23	121.5		
C21-O22-H24	55.9		
C21-O23-H24	106.3		
O23-H24-O22	76.3		

lowest bond length is 0.962 Å for O14-H28, which is due to the strong electronegativity of oxygen atom attached to it. This makes the O-H bonds shorter and stronger due to their high polarity. The bond lengths of C-O bonds present in 4HDA are 1.363 Å (21C-23O), 1.372 Å (6C-12O), 1.357 Å (5C-O10) and 1.369 Å (4C-9O), whereas for zingerone, they are 1.366 Å (2C-O5) and 1.381 Å (9C-O14), respectively. These shortened bond lengths are also due to the electronegative oxygen atoms attached to it. These reactive sites may be the suitable sites for protein interactions. The bond lengths of C-C, O-H and C-O in 4HDA and zingerone are consistent with the standard values, *e.g.* 1.54 Å for C-C, 0.96 Å for O-H, and 1.42 Å for C-O, indicating the accurate structural optimization [30]. The calculated bond lengths suggest that both compounds have the ideal structural configuration which enhances their suitability for the biological activity and drug-like characteristics.

Bond angles of both compounds are observed to differ significantly as a result of hybridization. Highest bond angle of 156.8º observed in 4HDA at C17-O12-H11 is due to the methoxy group, while zingerone's highest angle of 122.5º at C3-C2-O5 is due to the ketone group. The smallest angles, 55.9º for 4HDA and 104.9º for zingerone, indicate steric effect. In this work, potential reactive sites that were identified may act as known interactions for the chosen protein, which can be analyzed by molecular docking, to confirm the biological activity of the compounds. Knowing the bond length and bond angle can help to understand reactivity and biological activity of compound.

Spectroscopic analysis: FT-IR and FT-Raman vibrational analysis of 4HDA and zingerone were identified using theoretical and experimental techniques. Potential energy distribution (PED) helps interpret molecular dynamics by determining the contributions of different vibrational modes to the total energy [31,32]. A scaling factor of 0.961 [33] is incorporated in the calculated value of FT-IR and FT-Raman, since the theoretical values are observed in a gaseous state, whereas the experimental values are observed in a solid state. The vibrational assignments are given in Table-2 and the FT-IR and FT-Raman spectra of 4HDA and zingerone are shown in Figs. 2 and 3, respectively. The oxygen-hydrogen (O-H), carbon-hydrogen (C-H), carbon-oxygen (C-O) and carbon-carbon (C-C) vibrations normally fall in the regions 3600-3400 cm^{-1} [34], 3100-3000 cm^{-1} [35], 1740-1660 cm^{-1} [36], 1400-1650 cm^{-1} [37], respectively. Prominent vibrations of 4HDA and zingerone are discussed as follows:

TABLE-2
THEORETICAL AND EXPERIMENTAL VIBRATIONAL FREQUENCY OF 4HDA AND ZINGERONE

Modes	Experimental		Theoretical		IR intensity		Raman activity		Assignments PED (%)
	FT-IR	FT-Raman	Unscaled	Scaled[a]	Relative	Absolute[b]	Relative	Absolute[c]	
4HDA									
66			3776	3628	103	24	149	53	ν OH (100)
65			3758	3611	145	34	85	30	ν OH (100)
64			3232	3106	2	0	45	16	ν CH (99)
63		3033	3213	3088	2	1	57	20	ν CH (100)
62			3141	3019	17	4	117	41	ν CH (90)
61			3135	3013	19	4	115	41	ν CH (98)
60	2938		3096	2975	27	6	58	20	ν CH (100)
59		2942	3081	2961	28	7	49	17	ν CH (100)
58			3018	2900	27	6	283	100	ν CH (99)
57			3017	2900	83	19	17	6	ν CH (84)
56		1697	1781	1712	429	100	163	57	ν OC (82)
55		1592	1640	1576	89	21	50	18	ν CC (41) + β CCC (15)
54	1517		1630	1567	47	11	118	42	ν CC (70) + β HCC (11)
53			1529	1470	122	28	6	2	ν OC (15)
52	1457		1509	1450	8	2	7	3	β HCH (78) + τ HCOC (13)
51			1505	1446	62	14	6	2	β HCH (65) + τ HCOC (10)
50			1492	1433	11	2	12	4	β HCH (32) + β OCC (41) + τ HCOC (17)
49			1489	1431	16	4	13	5	β HCH (73) + τ HCOC (12)
48			1488	1429	35	8	2	1	β HCH (41)
47	1413		1481	1423	6	1	11	4	β HCH (72)
46	1371	1373	1452	1395	61	14	3	1	ν CC (14)
45			1413	1358	49	11	31	11	ν CC (22) + β HOC (21)
44	1318	1322	1365	1312	394	92	31	11	ν CC (13) + β HOC (20)
43	1245		1319	1267	129	30	25	9	ν OC (10) + β HOC (18) + β HCC (17)
42			1287	1237	86	20	3	1	ν CC (34) + β HOC (27) + β HCC (13)
41			1266	1216	9	2	1	0	ν OC (47)
40	1197	1195	1231	1183	205	48	3	1	ν OC (13) + β HCC (35)
39			1213	1166	25	6	5	2	β HCH (11) + τ HCOC (38)
38			1206	1159	17	4	9	3	β HCH (11) + τ HCOC (61)
37			1171	1126	1	0	2	1	β HCH (29) + τ HCOC
36			1171	1125	47	11	6	2	β HCH (25) + τ HCOC (64)
35			1169	1124	342	80	34	12	ν OC (16) + ν CC (12) + β HOC (30)
34	1103	1105	1126	1082	176	41	1	0	ν OC (37)
33		1032	1100	1057	104	24	5	2	ν CC (24) + ν OC (21) + β HCC (33)
32	904		1044	1004	93	22	19	7	ν OC (67)
31			931	895	14	3	6	2	ν OC (11) + ν CC (12) + β CCC (10) + τ HCCC (15)
30			931	894	30	7	1	0	ν OC (42) + τ HCCC (10)
29	863		919	883	9	2	1	1	ν OC (11) + τ HCCC
28		803	872	838	10	2	0	0	τ HCCC (73)
27	769		798	767	15	3	12	4	ν OC (22) + β CCC (25)
26			782	752	45	10	0	0	ω OCOC (68)
25			761	731	13	3	0	0	ω OCCC (69)
24	681	686	684	657	12	3	5	2	ν OC (13) + β OCO (24) + β OCC (10)
23			642	617	88	21	6	2	β OCO (33) + β OCC (11)
22			626	602	13	3	1	0	β COC (10) + ω OCCC (41)
21	579		601	577	32	8	1	0	τ HOCC (35) + τ CCCC (23)
20			552	530	12	3	3	1	β CCC (27) + β OCC (17)
19			531	510	52	12	2	1	τ HOCC (42) + τ CCCC (14)
18			524	503	4	1	2	1	β COC (11) + τ HOCC (10)
17			494	475	96	22	1	0	τ HOCC (93)
16			450	432	1	0	3	1	β OCC (26) + β COC (15)
15		380	384	369	2	0	1	1	β CCC (14) + β COC (15) + ω OCCC (27)

14			363	349	4	1	5	2	β CCC (16) + ω OCCC (11)
13			339	326	4	1	2	1	ν CC (31) + β HCC (21) + β OCC (10) + β COC (10)
12			317	304	4	1	3	1	β OCC (34) + β COC (10)
11		297	293	282	0	0	1	0	β OCC (30) + τ CCCC (11)
10			256	246	0	0	1	0	β COC (13) + τ HCOC (21)
9			229	220	1	0	1	0	β OCC (16) + β COC (12) + τ HCOC (10)
8			201	193	1	0	2	1	τ HCOC (10) + τ CCCC (35)
7			162	155	2	0	0	0	β OCC (12) + τ HCOC (37) + τ COCC (13)
6			146	140	0	0	1	0	β OCC (21) + β CCC49
5		122	129	124	1	0	1	0	τ CCCC (15) + τ COCC (15) + ω OCCC (20)
4		81	115	110	0	0	0	0	τ CCCC (38) + ω CCCC (31)
3			67	64	3	1	0	0	τ CCCC (10) + τ OCCC (15) + τ COCC (43)
2			63	60	6	1	1	0	τ COCC (72)
1			57	55	0	0	0	0	τ OCCC (69) + τ COCC (14)
Zingerone									
78			3841	3691	65	20	125	63	ν OH (100)
77		3067	3195	3070	4	1	74	38	ν CH (100)
76		3027	3172	3048	9	3	122	62	ν CH (93)
75			3138	3016	19	6	101	51	ν CH (93)
74			3130	3008	20	6	102	52	ν CH (100)
73	2998	2999	3120	2999	15	4	45	23	ν CH (99)
72			3114	2993	30	9	56	28	ν CH (100)
71	2959	2921	3104	2983	5	1	76	39	ν CH (100)
70	2938		3060	2940	16	5	27	14	ν CH (90)
69			3041	2922	71	21	197	100	ν CH (100)
68			3038	2919	5	1	179	91	ν CH (98)
67			3033	2915	11	3	146	74	ν CH (98)
66			3026	2908	4	1	62	32	ν CH (88)
65	2836		3003	2886	12	3	116	59	ν CH (98)
64	1703	1706	1779	1710	173	52	9	5	ν OC (90)
63	1600	1602	1653	1588	6	2	32	16	ν CC (49)
62	1521		1631	1568	92	28	16	8	ν CC (40) + β CCC (35)
61			1541	1481	133	40	3	1	ν CC (13) + β HCC (47)
60			1500	1442	31	9	6	3	β HCH (78) + τ HCOC (22)
59	1466		1491	1433	3	1	4	2	β HCH (72) + τ HCOC (19)
58	1454		1491	1433	8	2	14	7	β HCH (69)
57	1431		1482	1425	21	6	8	4	β HCH (55) + τ HCCC (28)
56			1478	1420	7	2	5	3	β HCH (78) + τ HCCC (15)
55	1409	1411	1477	1419	9	3	7	4	β HCH (74) + τ HCCC (21)
54			1457	1400	16	5	8	4	β HCH (50) + τ HCCC (16)
53	1367		1448	1391	28	8	1	1	ν CC (24) + β HCH (11)
52			1396	1342	48	15	8	4	β HCH (44)
51			1383	1329	31	9	1	1	β HCH (91)
50	1292	1294	1362	1309	8	2	8	4	ν CC (34) + β HOC (14) + β HCC (11)
49	1273		1330	1278	332	100	12	6	ν CC (13) + β HOC (12) + β HCC (30)
48			1319	1268	0	0	8	4	β HCC (57) + τ HCCC (25)
47	1250		1316	1265	87	26	22	11	ν OC (13) + ν CC (23) + τ HCCC (13)
46	1206		1267	1217	74	22	6	3	ν CC (13) + ν OC (12) + β HCC (31)
45	1191	1193	1252	1203	28	9	2	1	ν OC (25) + β HOC (11) + β HCC (13)
44			1212	1165	6	2	5	3	β HCH (13) + τ HCOC (56)
43	1154		1198	1152	0	0	0	0	β HCC (57) + τ HCCC (25)
42			1189	1143	35	11	6	3	ν CC (15) + β HOC (20) + β HCC (48)
41	1129		1183	1137	54	16	4	2	ν CC (18) + β HCC (11)
40			1166	1120	1	0	3	1	β HCH (26) + τ HCOC (72)
39			1158	1113	96	29	2	1	ν CC (27) + β OCC (15) + τ HCCC (24)
38			1121	1078	86	26	2	1	β CCC (11) + β HOC (16) + β HCC (15)

37	1034	1058	1075	1033	25	7	3	1	ν CC (43)
36			1073	1031	1	0	0	0	β HCC (29) + τ HCCC (24) + ω OCCC (12)
35	968		1064	1022	47	14	2	1	ν CC (15) + ν OC (33)
34	935		981	942	10	3	9	4	ν CC (41) + τ HCCC (32)
33			935	898	11	3	1	0	β HCC (10) + τ HCCC (23)
32			932	896	26	8	7	3	ν CC (27) + ν OC (23)
31	866		921	885	1	0	0	0	τ HCCC (85)
30	824		871	837	8	2	0	0	τ HCCC (45)
29	791	793	847	814	7	2	6	3	ν CC (42)
28			795	764	34	10	0	0	τ HCCC (74)
27	736		783	752	12	4	22	11	ν OC (20) + β CCC (27)
26	723	723	740	711	1	0	1	0	τ HCCC (29)
25			729	701	5	2	9	4	ν CC (10) + ν OC (10) + β CCC (46)
24	630		707	679	1	0	0	0	τ HCCC (25) + ω OCCC (36)
23			628	604	9	3	2	1	β CCC (14) + β OCC (33) + β COC (18)
22			592	569	5	2	7	4	ν CC (24) + β OCC (38)
21	542	563	584	561	7	2	0	0	τ HCCC (11) + τ CCCC (12) + ω OCCC (17) + ω OCCC (14)
20	505		506	486	13	4	4	2	β CCC (12) + β OCC (24)
19			491	472	0	0	0	0	τ CCCC (15) + ω OCCC (60)
18			485	466	4	1	3	1	β CCC (56)
17			467	449	6	2	0	0	τ HCCC (22) + τ CCCC (25) + ω OCCC (41)
16			414	398	1	0	1	1	β OCC (14) + β CCC (30)
15			347	333	11	3	3	1	β CCC (15) + β OCC (28) + β COC (38)
14			337	324	8	2	3	1	τ CCCC (20) + ω OCCC (30) + ω CCCC (22)
13			295	283	2	0	1	0	β OCC (36) + β CCC (27) + β COC (15)
12			248	239	2	0	3	2	β OCC (18) + β CCC (11) + β COC (15)
11			241	232	34	10	0	0	τ HOCC (37) + τ HCOC (15) + τ COCC (10)
10			210	201	60	18	3	1	τ HOCC (55)
9			192	184	0	0	1	0	τ HCOC (20) + τ CCCC (19) + ω OCCC (22) + ω CCCC (11)
8			190	182	6	2	1	1	β OCC (10) + β CCC (66)
7			128	123	3	1	1	0	τ CCCC (73)
6			112	107	0	0	0	0	τ HCCC (10) + τ CCCC (45) + ω CCCC (10)
5		71	76	73	3	1	0	0	β CCC (86)
4			43	41	3	1	1	0	τ CCCC (81)
3			-18	-17	3	1	1	0	τ CCCC (62) + ω CCCC (12)
2			-74	-71	6	2	0	0	τ HOCC (10) + τ COCC (72)
1			-93	-90	1	0	1	0	τ HCCC (80)

ν - stretching, β - in plane bending, ω - out of plane bending, τ - torsion. [a]Scaling factor 0.961 for B3LYP/6-311++G(d,p) basis set. [b]Relative absorption intensities normalized with highest peak absorption equal to 100. [c]Relative Raman intensities normalized to 100.

O-H vibration: O-H stretching vibrations of 4HDA and zingerone vibrate in the range 3628 cm^{-1}, 3611 cm^{-1} and 3691 cm^{-1}, with potential energy distribution (PED) 100%. When the PED reaches 100% for a specific normal mode, it signifies that the vibration is purely due to stretching motion, with no involvement from other vibrations.

C-H vibration: C-H vibrations of methoxy groups and aromatic ring of 4HDA fall in the region 3106-2900 cm^{-1} whereas zingerone vibrates between 3070-2886 cm^{-1} with the PED 84-100%. In contrast, the experimental wavenumbers of 4HDA fall in the range 2938 cm^{-1} (FT-IR) and 3033, 2942 cm^{-1} (FT-Raman), whereas zingerone fall in the range 2998, 2959, 2938, 2836 cm^{-1} (FT-IR) and 3067, 3027, 2999, 2921 cm^{-1} (FT-Raman), respectively.

C-O vibration: C-O stretching vibrations of a carboxyl group and methoxy group of 4HDA vibrates between 1712-1004 cm^{-1} with PED 15-82%. In case of zingerone, ketone group (C=O) typically shows a strong stretching vibration around 1700 cm^{-1} [38] due to the C=O bond, which is a characteristic feature of carbonyl compounds. C=O present in zingerone vibrates at 1710 cm^{-1} with a PED of 90%, In contrast, the experimental wavenumbers of 4HDA and zingerone also compliment the theoretical values.

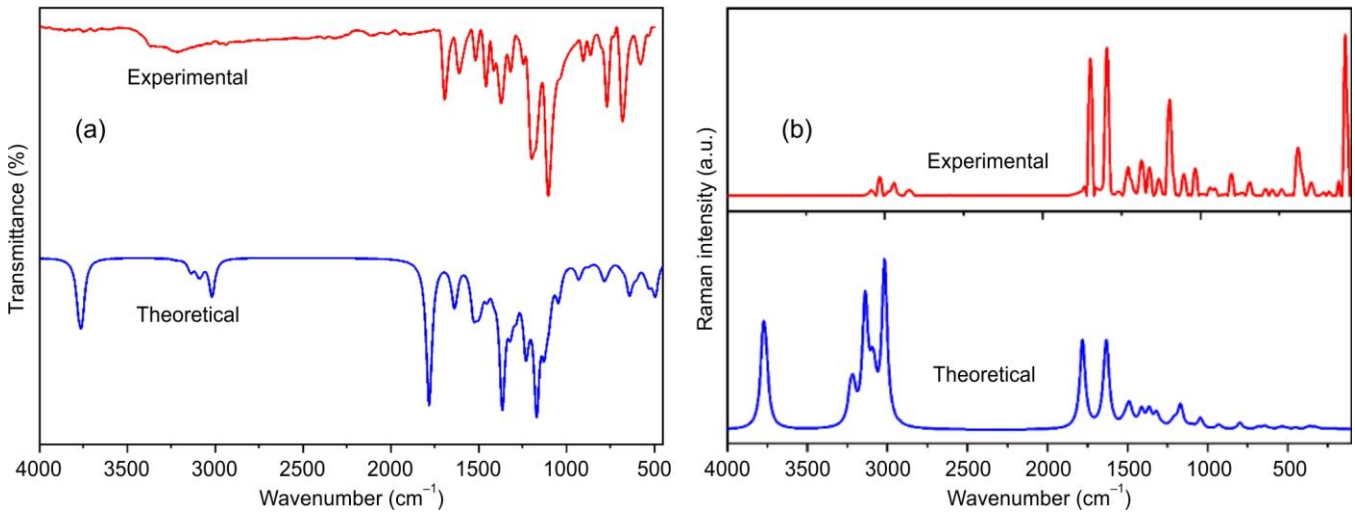

Fig. 2. Theoretical and experimental (a) FT-IR and (b) FT-Raman spectra of 4HDA

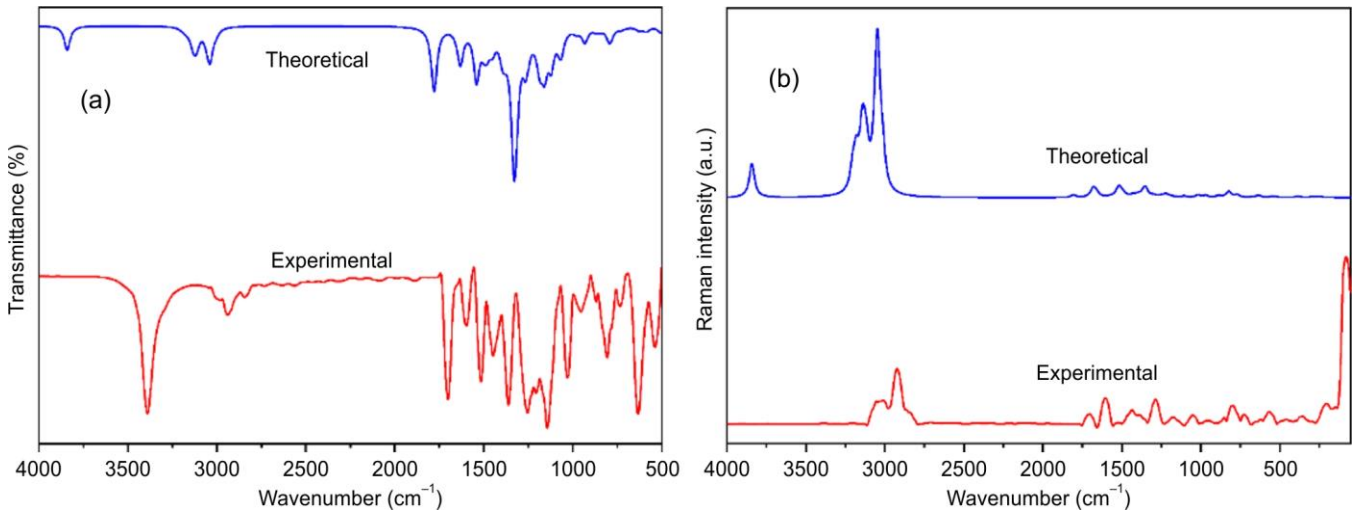

Fig. 3. Theoretical and experimental (a) FT-IR and (b) FT-Raman spectra of zingerone

C-C vibration: C-C present in the benzene ring of 4HDA falls in the region 1395 cm^{-1} with PED 14%, whereas zingerone vibrates at 1588 cm^{-1} with PED 49%. In contrast, the experimental wavenumbers of 4HDA fall in the range 1371 cm^{-1} (FT-IR) and 1373 cm^{-1} (FT-Raman) and zingerone falls in 1600 cm^{-1} (FT-IR) and 1602 cm^{-1} (FT-Raman), respectively.

Electronic properties

UV-Vis analysis: Table-3 presents the theoretical UV absorption values of 4HDA and zingerone. Fig. 4 presents the theoretical UV-visible spectrum of 4HDA and zingerone. In the electromagnetic spectrum, the wavelength of UV region lies in the range of 10–400 nm and the visible region extends from 400–600 nm [39]. The calculated wavelength of 4HDA is 274 nm and zingerone is 272 nm, which falls in the mid-UV region. According to the UV-visible spectral analysis, the electron absorption is associated with the transition from the ground state to the first excited state. It is mainly caused by an electron excitation from the highest occupied molecular orbital (HOMO) to the lowest unoccupied molecular orbital

TABLE-3
ELECTRONIC EXCITATIONS OF 4HDA AND ZINGERONE OBTAINED BY TD-DFT B3LYP/6-311++G(d,p) METHOD

Energy (cm^{-1})	Wavelength (nm)	Oscillatory strength	Assignments
		4HDA	
34918	286	0.1103	H-1->LUMO (33%), HOMO->LUMO (59%)
36489	274	0.1979	H-1->LUMO (53%), HOMO->LUMO (37%)
41124	243	0.0004	H-3->LUMO (53%), H-2->LUMO (43%)
		Zingerone	
36291	276	0.017	HOMO->LUMO (95%)
36653	272	0.0001	H-2->LUMO (94%)
38504	260	0.0541	H-1->L + 3 (11%), HOMO->L + 1 (80%)

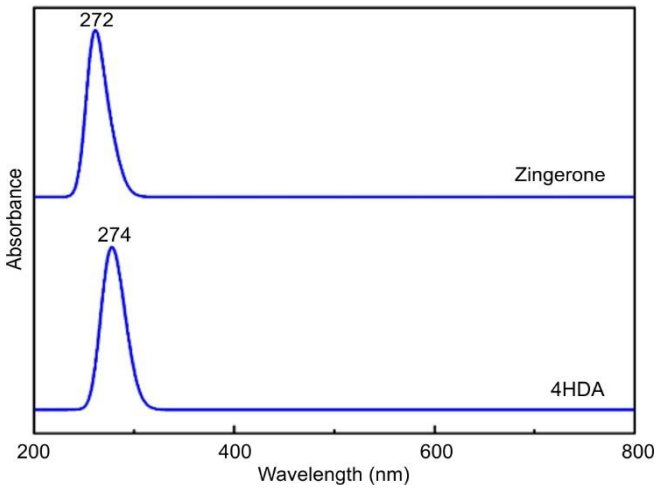

Fig. 4. Theoretical UV-visible spectrum of 4HDA and zingerone

(LUMO) [40]. Since 4HDA and zingerone wavelengths fall in the mid-UV region, only moderate energy is needed for this electronic transition, indicating moderate stability and moderate reactivity of both compounds.

Frontier molecular orbitals (FMO): Table-4 provides the HOMO-LUMO energy values and Fig. 5 display the HOMO-LUMO plot of 4HDA and zingerone. HOMO-LUMO energy difference gives the band gap value of 4HDA and zingerone, which is an important parameter in comprehending stability and reactivity of the molecule. Higher reactivity is indicated by a smaller HOMO-LUMO gap, whereas higher stability and lower reactivity are suggested by a larger HOMO-LUMO gap [41,42]. From the UV analysis, it is observed that 4HDA and zingerone absorption peaks lie in the mid-UV region, indicating that both compounds are moderately stable and moderately reactive. From the HOMO and LUMO energy the band gap of 4HDA is 4.7662 eV, while zingerone is 5.0135 eV. Using $E = hc/\lambda$, the absorption wavelengths for 4HDA and zingerone were found to be 260 nm and 247 nm, respectively, which matches the result obtained in the UV analysis indicating moderate stability and moderate reactivity of both compounds.

Table-4 shows the FMO energy parameters of 4HDA and zingerone, and highlighed that the compounds are less toxic in nature. It is also observed that both compounds have an electrophilicity higher than 1.5 eV, indicating a strong electrophilic nature [43]. These properties suggest that both

TABLE-4
CALCULATED FRONTIER MOLECULAR ORBITAL (FMO) ENERGY PARAMETERS OF 4HDA AND ZINGERONE

Properties	B3LYP/6-311++G(d,p)	
	4HDA	Zingerone
E_{HOMO} (eV)	-6.4818	-5.9006
E_{LUMO} (eV)	-1.7156	-0.8871
Ionization potential (I)	6.4818	5.9006
Electron affinity (A)	1.7156	0.8871
Energy gap (eV)	4.7662	5.0135
Electronegativity (χ)	4.0987	3.3938
Chemical potential (μ)	-4.0987	-3.3938
Chemical hardness (η)	2.3831	2.5067
Chemical softness (S)	0.2098	0.1995
Electrophilicity index (ω)	3.5247	2.2974

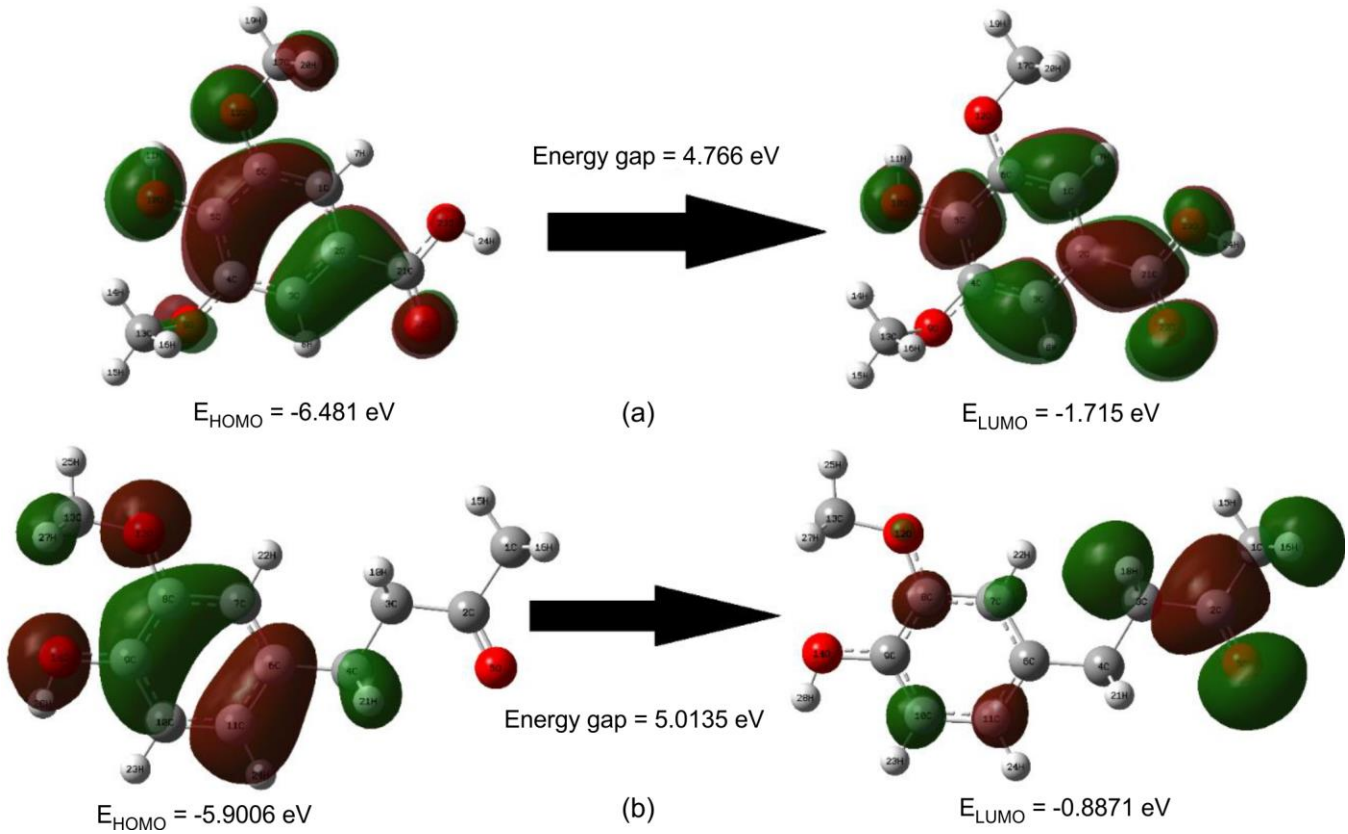

Fig. 5. HOMO-LUMO plots of (a) 4HDA and (b) zingerone

compounds are moderately stable and moderately reactive, which is consistent with their biological activities and contribute to its potential therapeutic applications.

Transition density matrix: Transition density matrix is an important analysis for studying the distribution of electrons in the excited states of a compound and to highlight its important electron density variation taking place during transitions [44]. High excitation densities, are shown in red colour and blue zones indicates lower excitation densities. 4HDA and zingerone TDM map for S1, S2 and S3 excited states are shown in Fig. 6. On comparing the excitation densities, which are shown in red colour, the excitation states 1, 2 and 3 for 4HDA, it can be observed that state 1 shows predominant excitation densities, indicating the highest charge transfer. In contrast, zingerone shows a greater concentration of red areas in the third excited state. Comparing both, 4HDA shows the maximum charge flow in the first state, while zingerone displays the maximum charge flow in the third state. From the energy values of these excited states, 4.326 eV for 4HDA (state 1) and 4.771 eV for zingerone (state 3), the wavelength can be calculated using the equation $E = hc/\lambda$. It is found to be 287 nm for 4HDA and 260 nm for zingerone, which falls in the mid-UV region, indicating that the moderate energy is needed for these transitions. This suggests moderate stability and moderate reactivity for both compounds, which is consistent with the results of UV and FMO analyses. These results emphasize their distinct electronic transitions and moderate stability of both compounds.

Topological analysis

Molecular electrostatic potential (MEP): Fig. 7 illustrates the MEP map of 4HDA and zingerone. Regions with negative potential, represented in red, indicate electron-rich areas and are linked to oxygen atoms in the hydroxyl and carbonyl groups of 4HDA and zingerone. O10, O9 and O22 of 4HDA and O14, O12 and O5 of zingerone are located in the red region. These regions are favourable for the electrophilic attack. In contrast, areas with positive potential, depicted in blue, are electron-deficient and commonly associated with hydrogen atoms. H11 of 4HDA and H28 of zingerone present in the blue region indicate nucleophilic attack since these hydrogen atoms are connected to the electronegative oxygen atoms, which was discussed in molecular geometry as well. These reactive sites are responsible for interactions with other molecules, such as proteins chosen for docking in the present study and may serve as suitable sites for the potential biological interactions.

Electron localization function (ELF) and localized orbital locator (LOL): Figs. 8 and 9 display the ELF and LOL maps of 4HDA and zingerone. The electron localization function (ELF) map of 4HDA and zingerone reveals areas of concentrated electron density, H19, H7, H11, H24 and H15 of 4HDA and H15, H28, H23 and H24 of zingerone are highlighted in red, showing high electron localization, leading to the maximum Pauli repulsion.

In contrast, lower electron localization areas, C17 and C21 of 4HDA and C9, C10, C11 and C13 of zingerone are

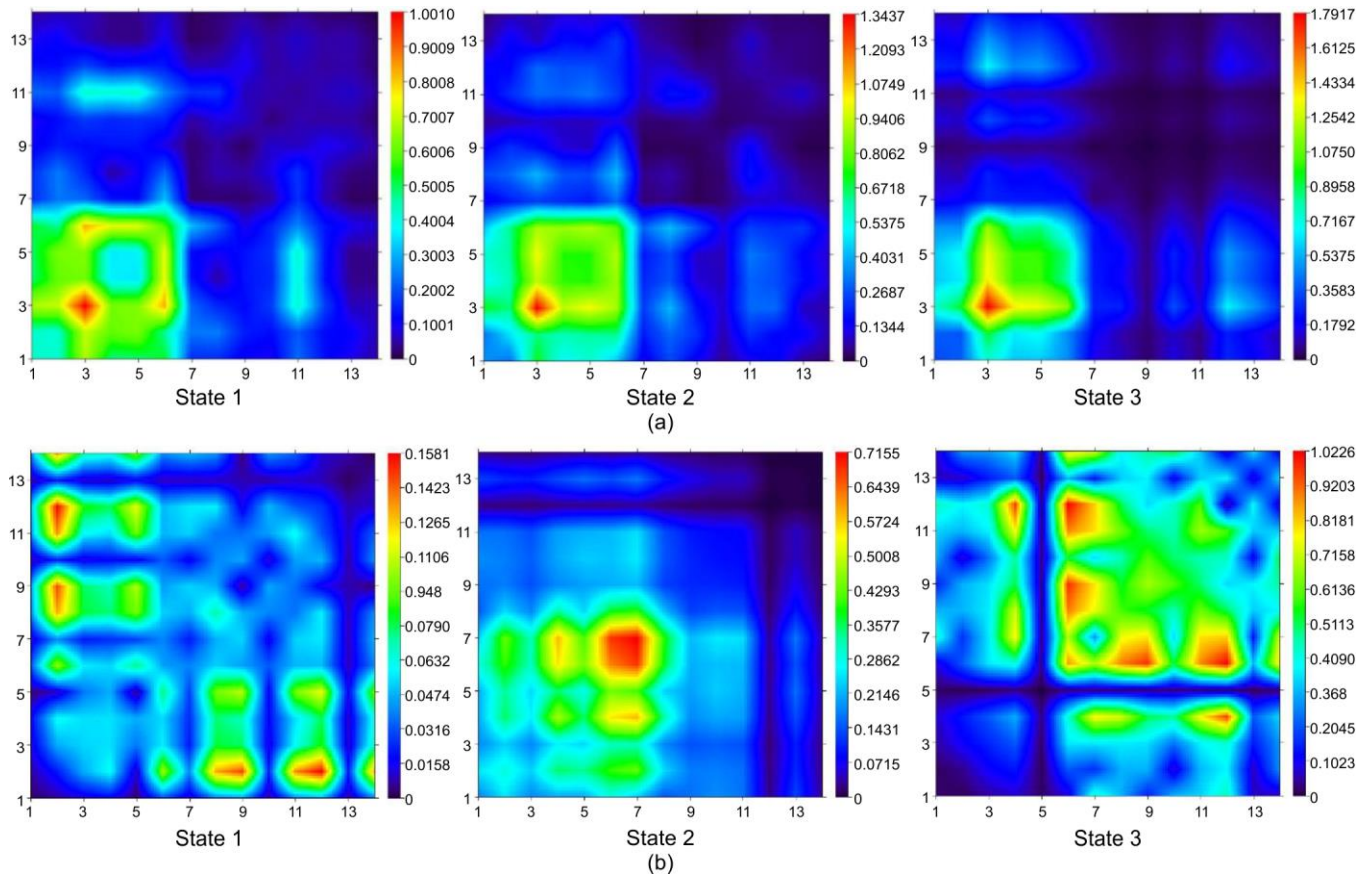

Fig. 6. TDM for S1, S2, S3 excited state of (a) 4HDA and (b) zingerone

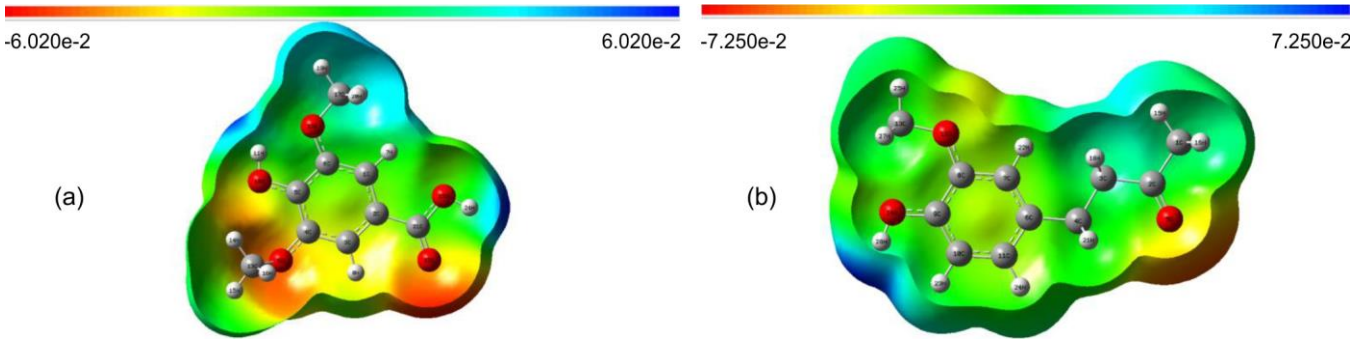

Fig. 7. Molecular electrostatic potential map of (a) 4HDA and (b) zingerone

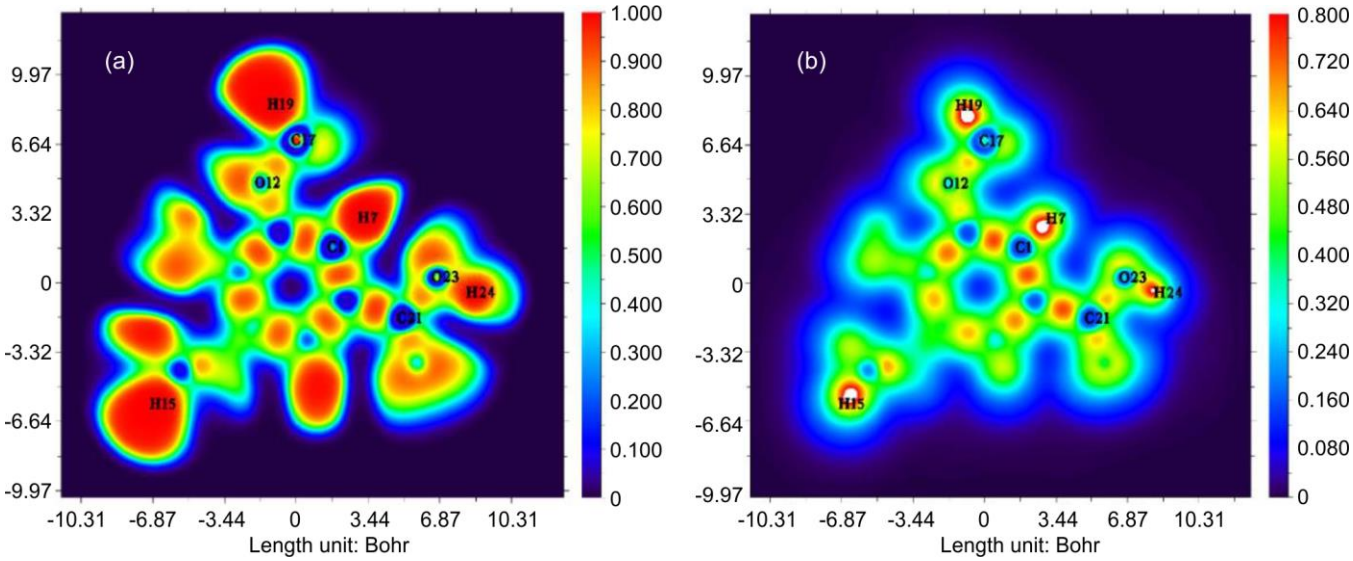

Fig. 8. (a) ELF and (b) LOL coloured filled maps of 4HDA

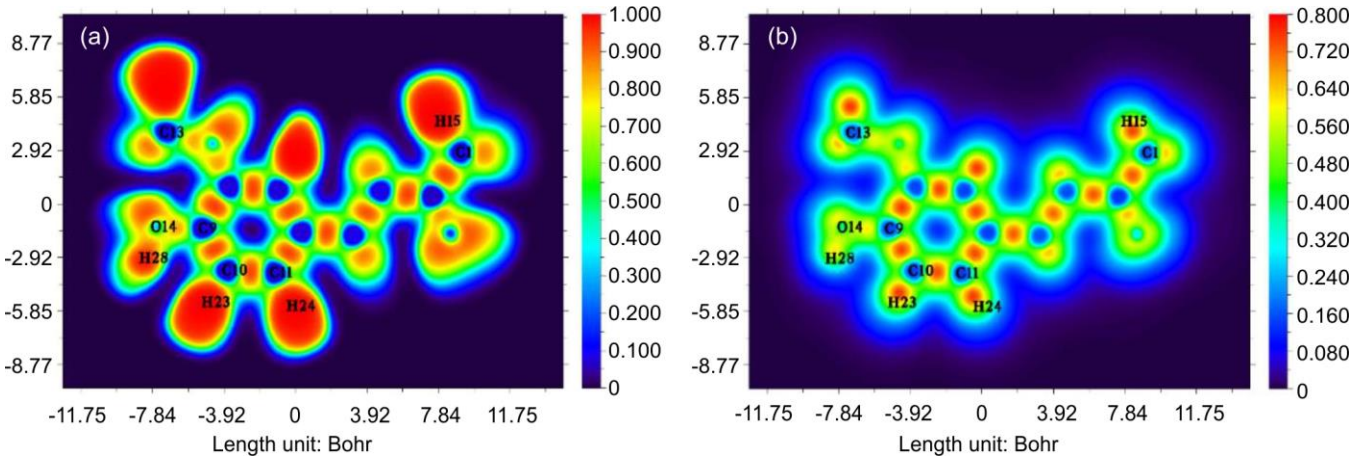

Fig. 9. (a) ELF and (b) LOL coloured filled maps of zingerone

highlighted in blue, leading to minimum Pauli repulsion. While the green regions represent areas of moderate electron density [45]. From the LOL map, it is observed that both compounds hydrogen atoms fall in the red region, indicating highly localized orbitals; similarly, carbon atoms fall in the blue region, indicating lower orbital localization. Thus, ELF and LOL complement each other by highlighting the distribution of electrons and the degree to which they are localized around atoms. MEP complements this by identifying charge-based reactive sites, highlighting the electron-rich and -deficient regions.

Reduced density gradient (RDG): Fig. 10 displays the RDG scatter plot of 4HDA and zingerone. Peaks in the blue region $\lambda_2 < 0$ of 4HDA and zingerone, indicating hydrogen bonding interactions. The presence of red spikes in the region $\lambda_2 > 0$ indicate steric repulsion caused by close atomic packing or electron cloud overlap. The prominent green spikes in the region $\lambda_2 \approx 0$ indicate weak non-covalent interactions of 4HDA

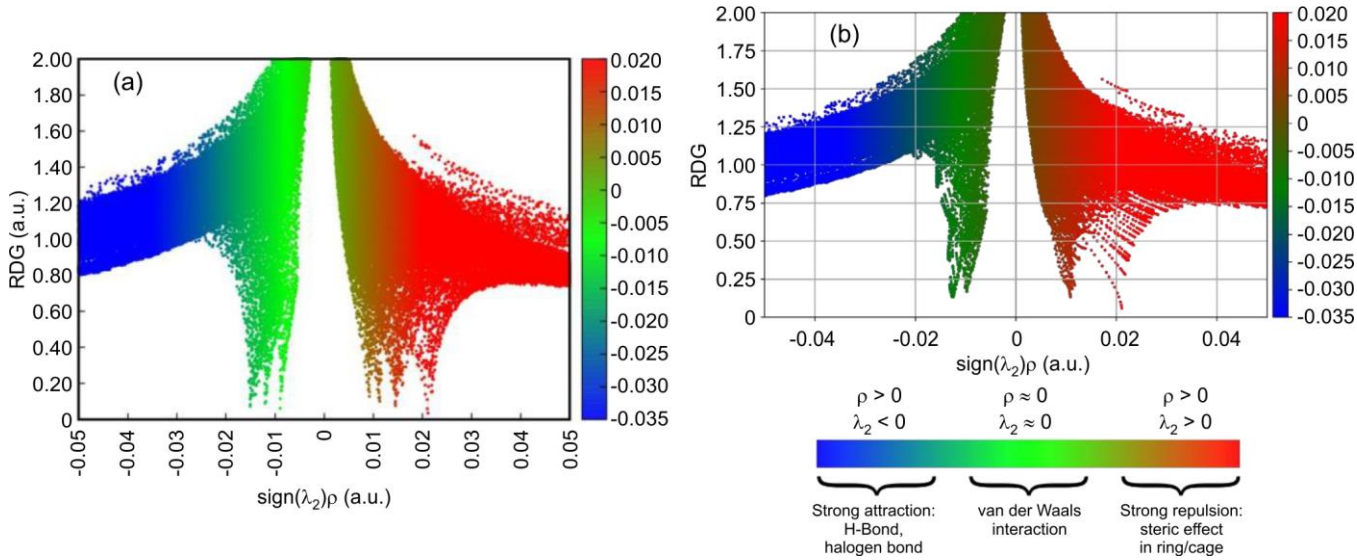

Fig. 10. RDG scatter maps of (a) 4HDA and (b) zingerone

and zingerone. These interactions are caused by weak van der Waals forces, which are gentle forces that keep molecules together without forming strong bonds and are crucial in stabilizing the molecular conformation [46]. The insights from RDG analysis reveal the molecular stability of 4HDA and zingerone, contributing to their functional roles in the biological systems, specifically by supporting stable complex formation during the docking analysis.

Biological analysis

ADMET properties: Desired limits and predicted values of ADMET properties for 4HDA, zingerone and mesalamine (standard drug) are mentioned in Table-5. It is observed that 4HDA has five hydrogen bond acceptors and two hydrogen bond donors, while zingerone has three hydrogen bond acceptors and one hydrogen bond donor, which fall within the optimal range, which is important for receptor binding. Zingerone and 4HDA have molecular weights of 194.23 and 198.17 g/mol, respectively, which fall within the ideal range of 500 g/mol. Topological polar surface area (TPSA) is the surface area of a compound occupied by polar atoms. TPSA values of 75.99 Å^2 for 4HDA and 46.53 Å^2 for zingerone are within the desired range, maintaining good membrane permeability. Zingerone has four rotatable bonds, whereas 4HDA has three, indicating intermediate molecular flexibility that permits receptor interactions without compromising the structural stability. WLogP stands for lipophilicity or the partition coefficient, which measures the extent to which a compound tends to dissolve in a fatty (lipophilic) environment and watery (hydrophilic) environment. Both compounds' WLogP values are 1.54 for 4HDA and 2.09 for zingerone, falling within the acceptable range of < 5, highlighting the favourable pharmacokinetic property of both compounds. Since both compounds are water soluble, the influence of toxicity due to solvent does not arise. Bioavailability score of 4HDA is 0.56 and zingerone is 0.55, which falls in the desired range of ≥ 0.55, indicating

TABLE-5
ADMET PARAMETERS OF 4HDA AND ZINGERONE

Parameters	Desired range	4HDA	Zingerone	Mesalamine (standard drug)
Hydrogen bond donor (HBD)	< 5	2	1	3
Hydrogen bond acceptor (HBA)	< 10	5	3	3
Polar surface area (TPSA) (Å^2)	40-130 Å^2	75.99 Å^2	46.54 Å^2	83.55 Å^2
Rotatable bonds	< 10	3	4	1
Molecular weight	< 500 g/mol	198.17 g/mol	194.23 g/mol	153.12 g/mol
WLOGP	< 5	1.54	2.09	0.28
Bioavailability score	≥ 0.55	0.56	0.55	0.56
GI absorption	–	high	high	high
Lipinski violation	–	0	0	0
Skin permeation	–	-6.77 cm/s	-6.70 cm/s	-6.30 cm/s
BBB permeant	–	No	Yes	No
Water solubility	–	Soluble	Soluble	Soluble
CYP1A2 inhibitor	–	No	No	No
CYP2C19 inhibitor	–	No	No	No
CYP2C9 inhibitor	–	No	No	No
CYP2D6 inhibitor	–	No	No	No
CYP3A4 inhibitor	–	No	No	No

both compounds' exhibit a probable high absorption during the administration of the desired treatment protocol. Similar to the standard drug mesalamine, the calculated drug like properties of 4HDA and zingerone are within the desired range, indicating good pharmacokinetic property.

A brief evaluation of 4HDA and zingerone pharmacokinetic properties was obtained with the SwissADME software's bioavailability radar, as shown in Fig. 11. The red line present in the bioavailability radar indicates the line that joins the different pharmacokinetic parameters. It is found that the line falls in the optimal range, which is depicted by the pink area indicating compound 4HDA and zingerone suitable for the biological activity [47]. BOILED egg plot was also observed, which shows the potential for intestinal absorption and blood brain permeability of 4HDA and zingerone. Boiled egg plot of both compounds is displayed in Fig. 12. As the white zone denotes an increased probability of absorption through the intestinal tract, the yellow zone implies a significant potential for brain permeability [48]. For 4HDA, the red circle is present in the white region, indicating 4HDA has good intestinal absorption, whereas for zingerone, the red circle is present in both the white and yellow regions, indicating zingerone can cross the blood-brain barrier and has good intestinal absorption as well, these results are also present in Table-5.

Blood-brain barrier (BBB) permeability results of 4HDA and zingerone indicate key differences of their therapeutic uses in the nervous system (Table-5). In case of 4HDA, which is impermeable to BBB indicates that 4HDA could be a potential candidate for treating peripheral nervous system (PNS) conditions like inflammation and pain management by sending the electrical signals through electrochemical reactions. In contrast zingerone is permeable to BBB, which allows it to address both central nervous system (CNS) and peripheral nervous system (PNS) related inflammations and also pain management. This property may also help to treat neurodegenerative disorders [49]. The high gastrointestinal (GI) absorption of 4HDA and zingerone indicates their efficient oral bioavailability, meaning they can be well absorbed into the bloodstream when taken orally. Potential metabolic stability and drug-drug interaction risks were examined through cytochrome P450 (CYP) enzyme inhibition results of 4HDA and zingerone. From Table-5, it is observed that both compounds

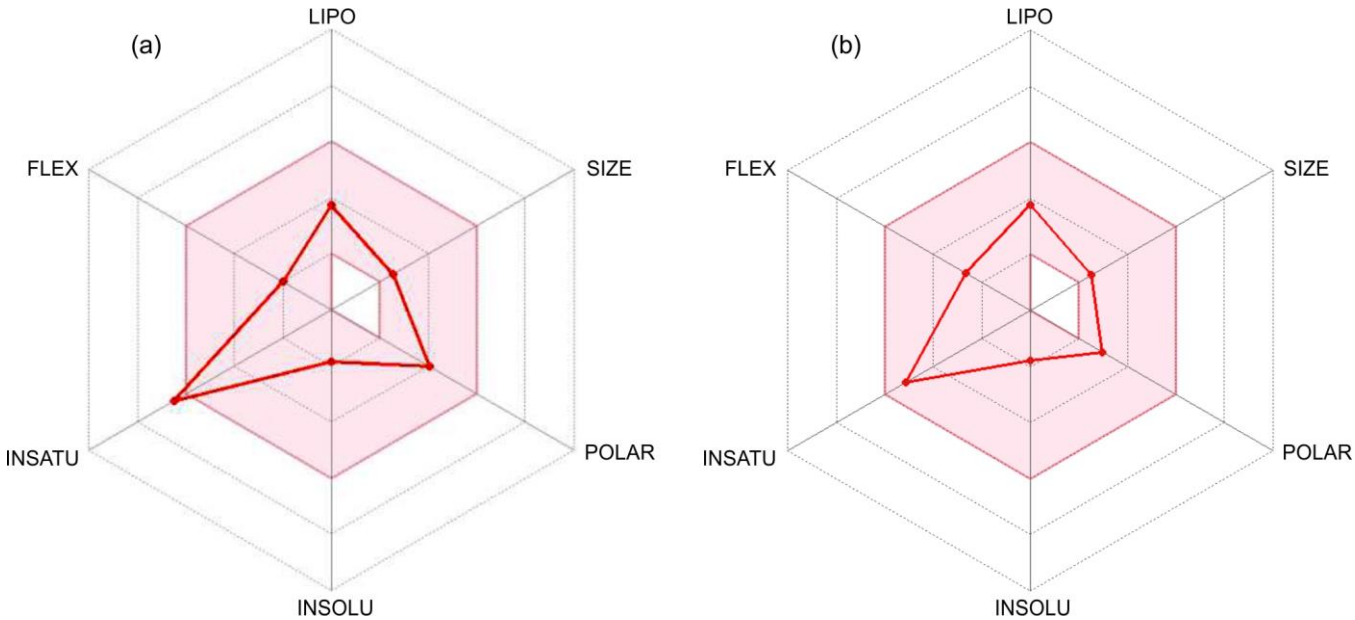

Fig. 11. Bioavailability radar of (a) 4HDA and (b) zingerone

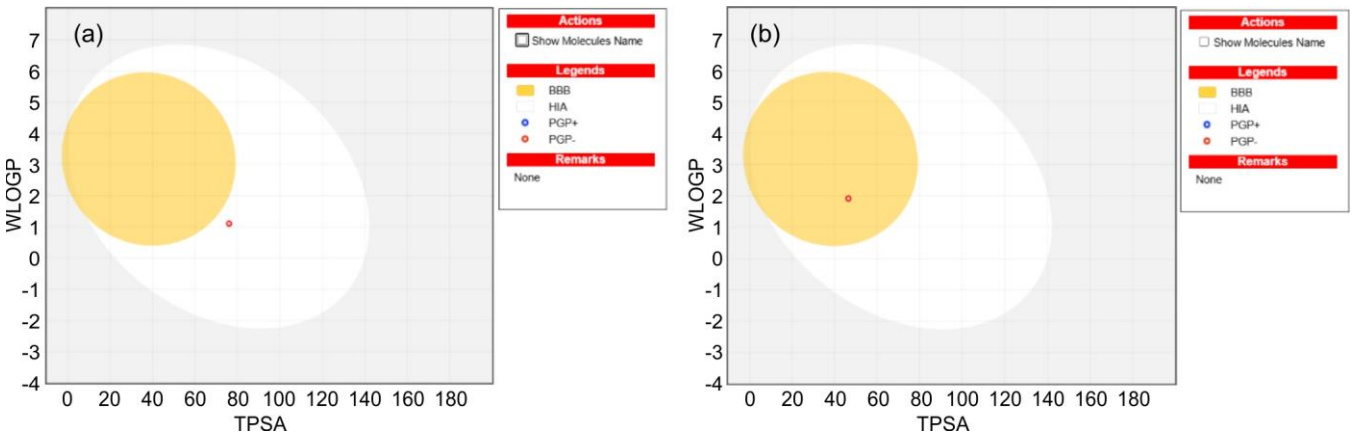

Fig. 12. Boiled egg plot of (a) 4HDA and (b) zingerone

does not inhibit CYP enzymes CYP1A2, CYP2C19, CYP2C9, CYP2D6 and CYP3A4, indicating a good metabolic stability and low drug interaction risk. For combination treatments, both compounds are a safer option because it does not affect drug metabolism. Collectively, the pharmacokinetic properties of 4HDA and zingerone indicate both compounds may be promising candidates for oral drug development.

Cytotoxicity: Both 4HDA and zingerone have concentration dependent cytotoxicity, with higher concentration cell viability decreasing and at lower concentrations cell viability increasing (Table-6). Half maximal inhibitory concentration (IC_{50}) values for 4HDA and zingerone are 370.7 ± 2.57 and 585.20 ± 2.58 µg/mL, respectively, confirming their therapeutic potential since they exhibit less toxicity. In order to understand the comparative analysis for the cytotoxicity for the chosen compounds the cell viability at 500 µg/mL is analyzed and found to be 14.14% for 4HDA and 51.95% for zingerone, respectively indicating zingerone is less toxic than 4HDA. However, at lower concentrations, both the compounds exhibit minimal toxicity with increased cell viability (Table-6). FMO studies also support the findings of toxicity analysis, predicting that the chosen compounds are less toxic in nature. From Figs. 13 and 14, it can be observed that the treated cells showed significant structural changes such as increased cellular rounding and reduced cell size attribute to the fact that both the title compounds are less toxic with a promising bioactivity.

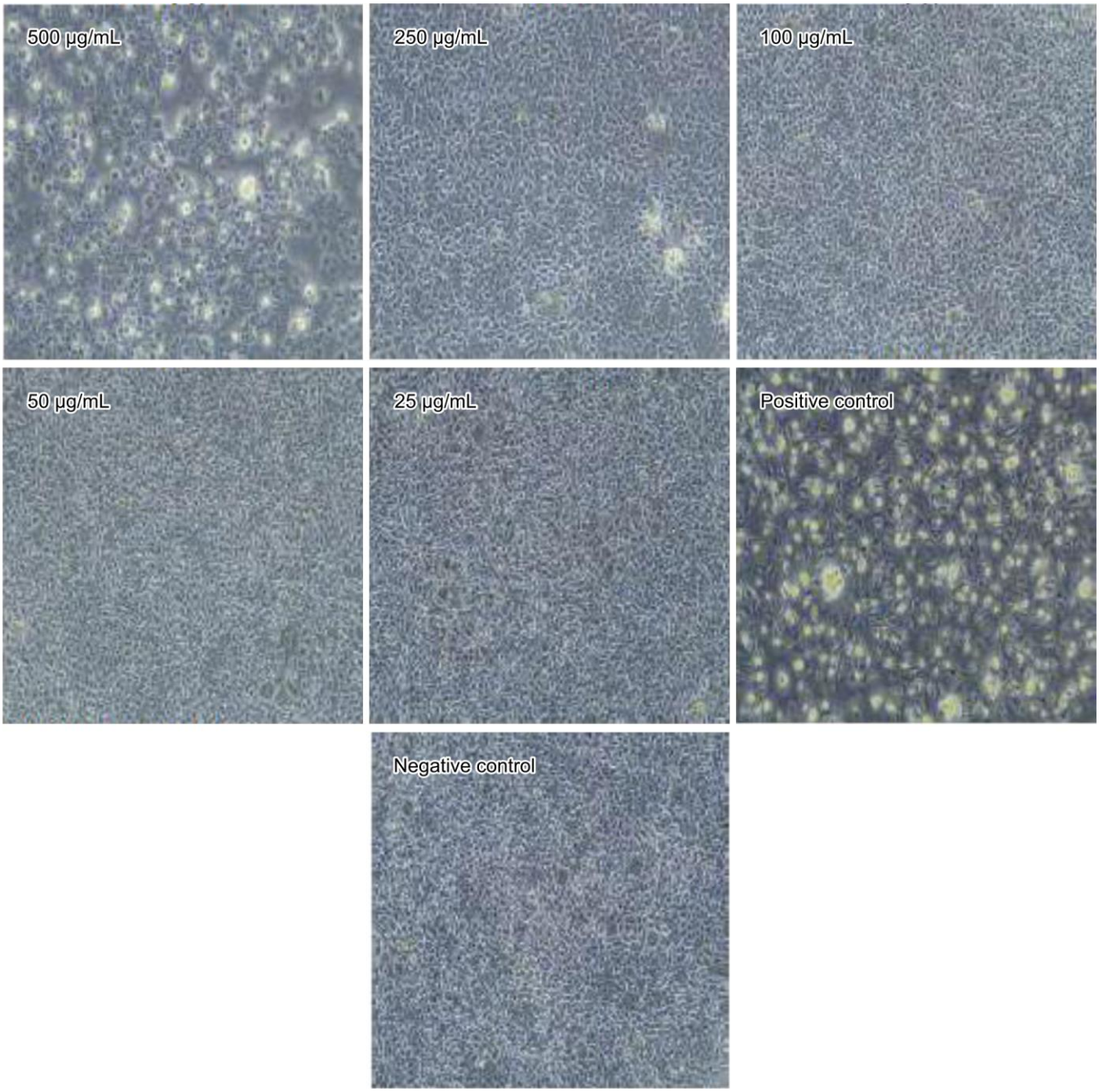

Fig. 13. Morphological alterations of the Vero cell line (L929) for various 4HDA concentrations

TABLE-6
CELL VIABILITY AT DIFFERENT
CONCENTRATION OF 4HDA AND ZINGERONE

Conc. (µg/mL)	4HDA		Zingerone	
	Absorbance 570 nm	% Cell viability (vero cell)	Absorbance 570 nm	% Cell viability (vero cell)
500	0.057	14.14	0.096	51.95
250	0.362	91.50	0.194	72.34
100	0.393	99.24	0.248	82.86
50	0.395	99.75	0.252	96.42
25	0.395	99.83	0.255	99.67
Negative control	0.396	100.00	0.256	100.00
Positive control	0.144	36.45	0.126	61.93

Ramachandran plot: Fig. 15 shows the Ramachandran plots of 2az5 (TNF alpha protein) and 2bxk (macrophage inflammatory protein 2). Ramachandran plot analysis of the 2az5 structure indicates that 90.2% of its residues fall within the most favoured region, which is a positive indicator of good structural stability and appropriate peptide backbone conformations. No residues fall in the forbidden region, which supports the protein 2az5 structural integrity. Furthermore, the Ramachandran plot of protein 2bxk indicates that 92.1% of its residues fall within the most favoured region and no residues in the forbidden region, which indicates stability of the protein 2bxk. Since both proteins have stable structural conformation, it is suitable for docking analysis.

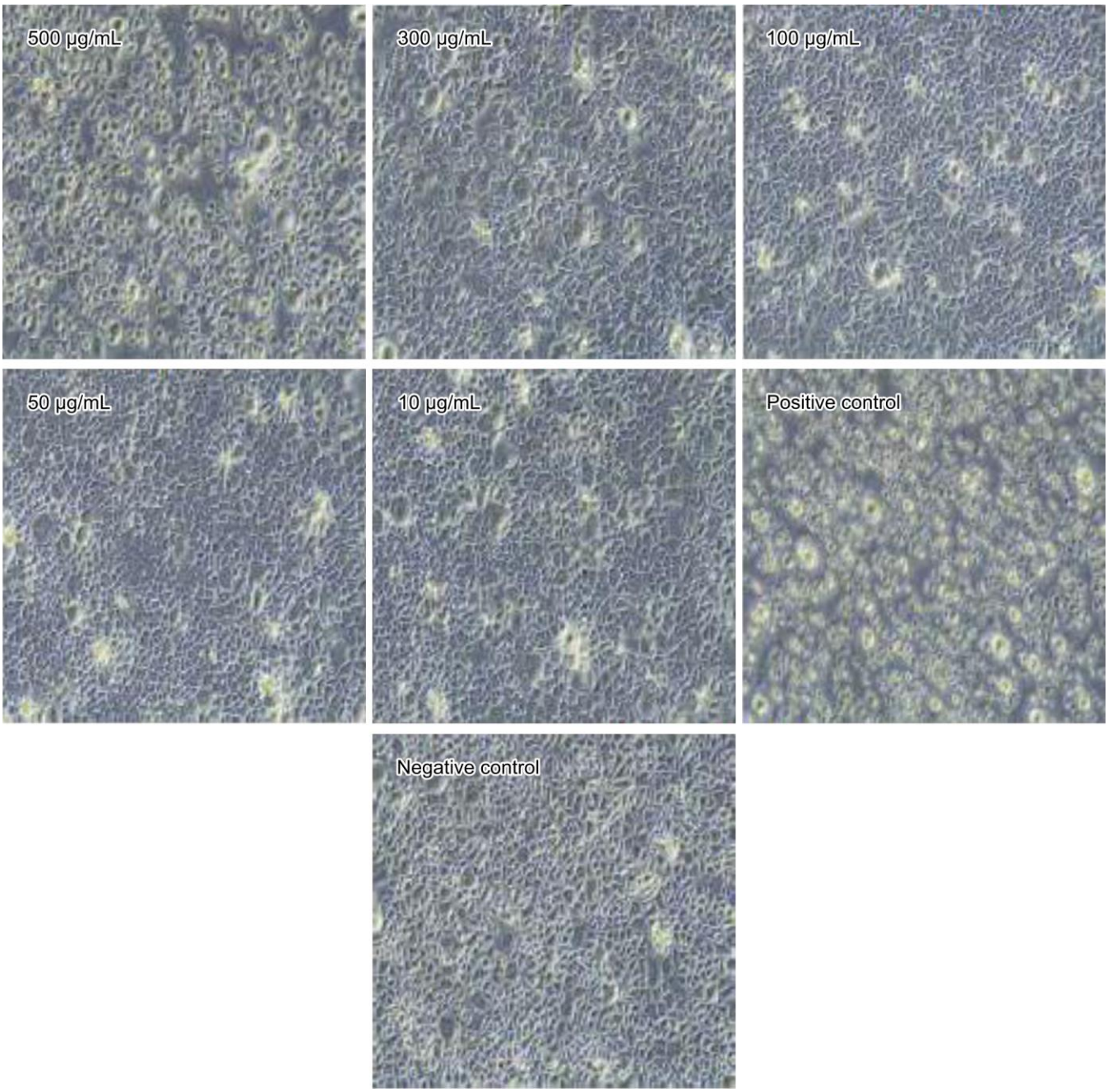

Fig. 14. Morphological alterations of the Vero cell line (L929) for various zingerone concentrations

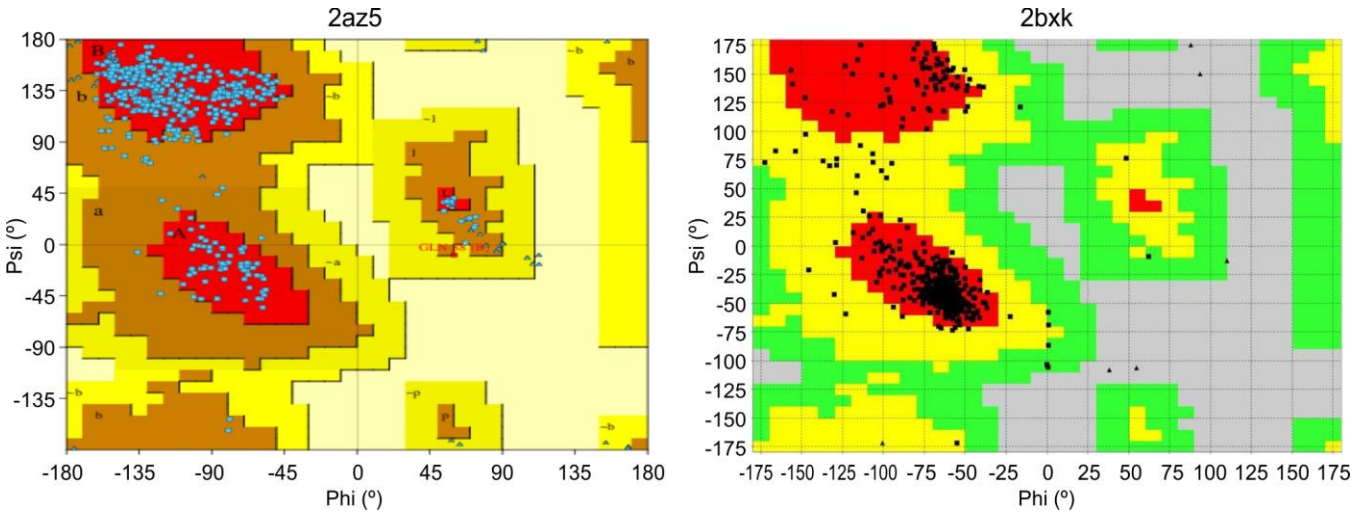

Fig. 15. Ramachandran plots of 2az5 protein (inflammatory bowel disease) and 2bxk protein (inflammatory)

Molecular docking: 4HDA and zingerone was docked against protein 2az5 and 2bxk, which is related to the inflammatory bowel disease and inflammation using AutoDock1.5.6. Table-7 outlines the docking parameters, whereas Figs. 16-18 illustrate the docking conformations of 4HDA, zingerone and mesalamine (standard drug) with proteins 2az5 and 2bxk, respectively.

From Table-7, it is observed that 4HDA interacts with ALA-156, ASP-10, LYS-11 and ASN-39 residues of 2az5 to form six hydrogen bonds with -4.65 kcal/mol binding affinity, while zingerone interacts with ALA-134, TRP-28, ILE-136 and ASN-46 residues to form four hydrogen bonds with a greater binding affinity of -5.39 kcal/mol. Against 2bxk, 4HDA forms four hydrogen bonds with a binding affinity of -4.2 kcal/mol with LYS 414, SER 489 and ARG 410, whereas zingerone forms a single hydrogen bond with LEU-66 with a binding affinity of -4.58 kcal/mol. In contrast, mesalamine (standard drug), which shows lower binding affinities of -3.4 kcal/mol for 2az5 and -3.67 kcal/mol for 2bxk, indicates that the binding affinities of 4HDA and zingerone with 2az5 and 2bxk are better when compared with the binding affinity of the standard drug mesalamine. The interactions of 4HDA and zingerone with proteins 2az5 and 2bxk show the binding interactions at specific atoms. Protein 2az5 and 2bxk interact

TABLE-7
MOLECULAR DOCKING PARAMETERS OF 4HDA AND ZINGERONE

Protein	Compound name	Bonded residues	Bond distance (Å)	Inhibition constant	Binding energy (Kcal/mol)
2az5 (Inflammatory bowel disease)	4HDA	ALA-156	2.2	391.6	-4.65
		ASP-10	1.9		
		ASP-10	1.8		
		LYS-11	2.3		
		LYS-11	2.3		
		ASN-39	2.7		
	Zingerone	ALA-134	2.1	111.8	-5.39
		TRP-28	2.3		
		ILE-136	1.8		
		ASN-46	1.9		
	Mesalamine (standard drug)	LEU-75	1.9	3.24	-3.4
		LEU-75	2.4		
		HIS-73	2.1		
		HIS-73	2.0		
2bxk (Inflammatory)	4HDA	LYS 414	2.4	839.36	-4.2
		SER 489	2.2		
		ARG 410	2.5		
		ARG 410	2.8		
	Zingerone	LEU-66	2.0	439.99	-4.58
	Mesalamine (Standard drug)	LEU-481	2.1	2.04	-3.67
		SER-454	2.2		
		SER-454	2.1		
		ARG-484	2.6		
		ARG-484	2.2		

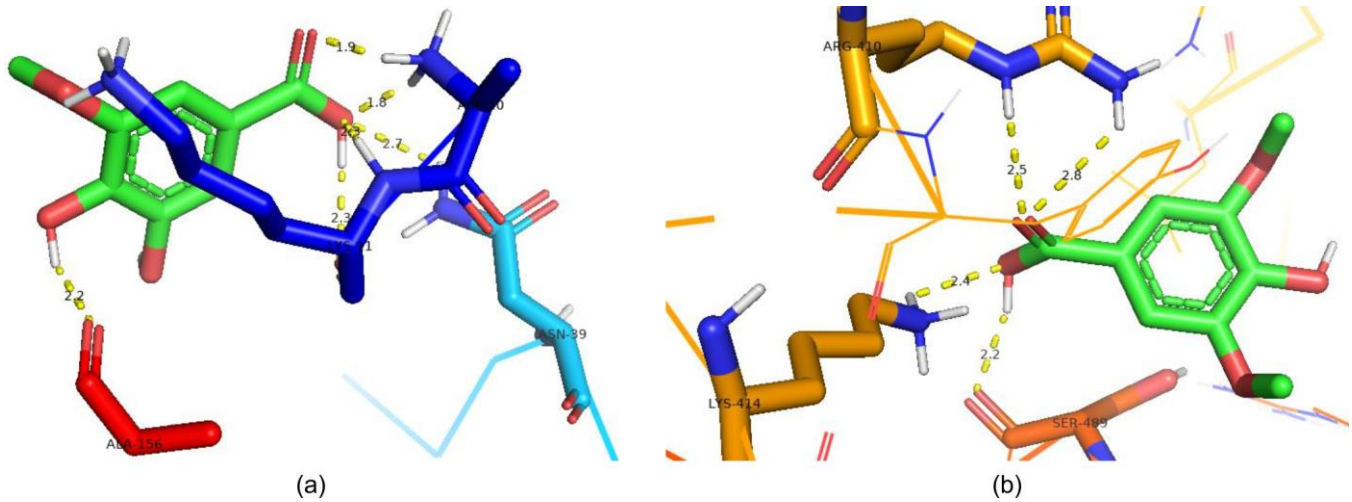

Fig. 16. Docking conformation of the ligand 4HDA with (a) 2az5 protein (inflammatory bowel disease) and (b) 2bxk protein (inflammatory)

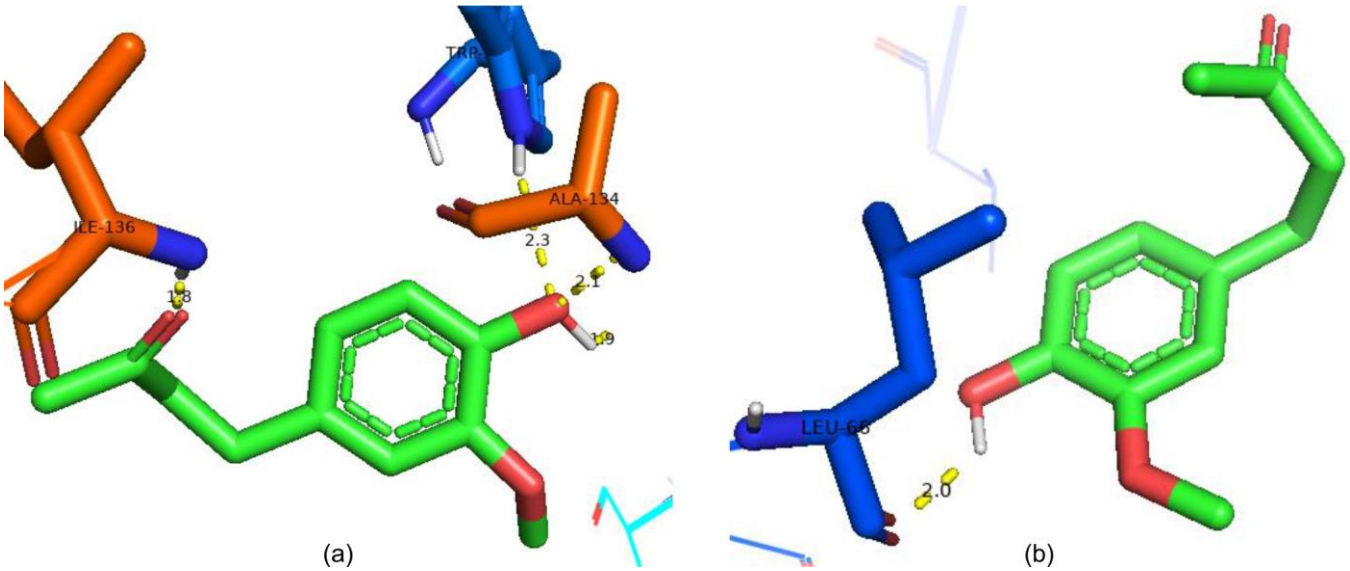

Fig. 17. Docking conformation of the ligand zingerone with (a) 2az5 protein (inflammatory bowel disease) and (b) 2bxk protein (inflammatory)

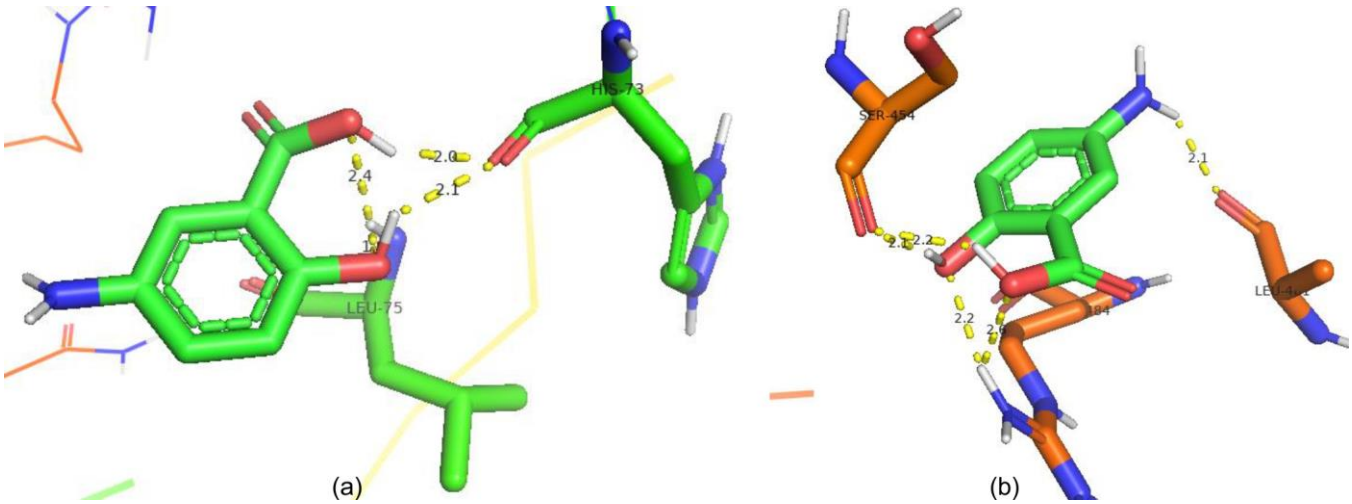

Fig. 18. Docking conformation of the standard drug (mesalamine) with (a) 2az5 protein (inflammatory bowel disease) and (b) 2bxk protein (inflammatory)

with the H11 atom of 4HDA due to the electronegative oxygen atom attached to it. Similarly, both proteins interact with H28 atom of zingerone due to the oxygen influence.

In light of docking studies to understand the interactions between the title compounds and the chosen proteins fall in line with the geometric analysis and MEP studies. Molecular geometry analysis of 4HDA and zingerone, indicates the role of electronegative oxygen atoms that are attached to H11 of 4HDA and H28 of zingerone in protein-ligand interactions. Also, MEP analysis indicates that H11 atom of 4HDA and H28 atom of zingerone are responsible for interaction with the potential sites of proteins, as these hydrogen atoms are prone to attack electron-rich regions of the proteins since they are attached to electronegative oxygen atoms O10 and O14, respectively. From drug likeness, it is observed that both compounds have high gastrointestinal absorption, which makes the compounds interact well with the gastrointestinal-related disease inflammatory bowel disease (IBD). Molecular docking results are consistent with the other biological parameters, which predict that 4HDA and zingerone have favourable protein-ligand interactions and may therefore be used as therapeutic medication for inflammatory bowel disease (IBD).

Conclusion

In present study, the optimized structure, vibrational spectroscopy, electron density analysis, reactive sites and pharmaceutical activities of 4-hydroxy-3,5-dimethoxybenzoic acid (4HDA) and zingerone were analyzed using DFT and molecular docking analyses. Through optimization, the structural stability and potential reactive sites for protein interactions of each compound were found. Shorter bond lengths of 0.968 Å (O10-H11) in 4HDA and 0.962 Å (O14-H28) in zingerone are due to the electronegative oxygen atom attached to it. These reactive sites may be the suitable sites for protein interactions. FT-IR and FT-Raman spectroscopy analyses were carried out theoretically and experimentally, which determined the existence of functional groups in 4HDA and zingerone. A scaling factor of 0.961 is incorporated in the theoretical values since they are observed in a gaseous state, whereas the experimental values are observed in a solid state. The O-H stretching vibrations are observed at 3628 cm^{-1} for 4HDA and 3691 cm^{-1} for zingerone with a PED of 100%, indicating it is pure stretching vibration, whereas experimental O-H stretching vibration observed at 3392 cm^{-1}, respectively. Pure C-H vibrations of 4HDA and zingerone observed at 3033 cm^{-1} and 3070 cm^{-1}, whereas experimental values were observed at 3088 cm^{-1} and 3067 cm^{-1}, respectively. The experimental and theoretical vibrational spectroscopic values of both compounds are in line with each other. The calculated UV absorption wavelengths for 4HDA and zingerone are 274 nm and 272 nm, respectively, while FMO analysis predicts values of 260 nm for 4HDA and 247 nm for zingerone. These wavelengths fall within the mid-UV region, indicating moderate molecular stability and reactivity. Softness values of 0.2098 (4HDA) and 0.1995 (zingerone), both below the threshold of < 2, suggest low toxicity. High electrophilicity values of 3.5247 for 4HDA and 2.2974 for zingerone (both >1.5 eV) confirm strong electrophilic nature. Transition density matrix (TDM) excitation maps indicate the maximum charge transfer at excited state 1 for 4HDA (287 nm) and state 3 for zingerone (260 nm), placing both in the mid-UV region, consistent with UV and FMO analyses, confirming moderate stability and reactivity. MEP maps identify the nucleophilic regions at H11 (4HDA) and H28 (zingerone), due to their bonding with electronegative oxygen atoms. ELF and LOL analyses show high electron localization (red regions) around specific hydrogen atoms in both molecules, indicating regions of maximum Pauli repulsion, while blue regions near selected carbon atoms correspond to the minimum repulsion, with both maps in strong agreement. RDG analysis reveals significant non-covalent interactions, notably van der Waals forces, which enhance the molecular stability. Combined surface analyses (MEP, ELF, LOL, RDG) suggest potential binding interactions relevant to biological activity. ADMET profiling, including Lipinski's rule of five, water solubility, bioavailability, BBB penetration, GI absorption and metabolic stability, shows that both compounds possess favourable pharmaco-kinetic properties, comparable to the standard drug mesalamine. MTT assay results indicate IC_{50} values of 370.7 ± 2.57 μg/mL for 4HDA and 585.2 ± 2.58 μg/mL for zingerone, supporting their therapeutic potential. Ramachandran plot analysis confirms the structural stability of target proteins (2az5 and 2bxk), validating their use in docking studies. Molecular docking shows higher binding affinities for 4HDA and zingerone with 2az5 (-4.65 and -5.39 kcal/mol) and 2bxk (-4.2 and -4.58 kcal/mol), compared to mesalamine (-3.4 and -3.67 kcal/mol), indicating stronger interactions. These results, supported by physico-chemical, pharmacokinetic and biological analyses, suggest that 4HDA and zingerone are promising candidates for the treatment of inflamematory bowel disease (IBD).

CONFLICT OF INTEREST

The authors declare that there is no conflict of interests regarding the publication of this article.

REFERENCES

1. J.M. Pezzuto, *J. Agric. Food Chem.*, **56**, 6777 (2008); https://doi.org/10.1021/jf800898p
2. L.A. Pacheco-Palencia, S. Mertens-Talcott and S.T. Talcott, *J. Agric. Food Chem.*, **56**, 4631 (2008); https://doi.org/10.1021/jf800161u
3. K. Kim, R. Tsao, R. Yang and S. Cui, *Food Chem.*, **95**, 466 (2006); https://doi.org/10.1016/j.foodchem.2005.01.032
4. J. Ji, X. Yang, M. Flavel, Z.P.-I. Shields and B. Kitchen, *J. Am. Coll. Nutr.*, **38**, 670 (2019); https://doi.org/10.1080/07315724.2019.1587323
5. C.M. Guimarães, M.S. Gião, S.S. Martinez, A.I. Pintado, M.E. Pintado, L.S. Bento and F.X. Malcata, *J. Food Sci.*, **72**, 1 (2007); https://doi.org/10.1111/j.1750-3841.2006.00231.x
6. M.A. Deseo, A. Elkins, S. Rochfort and B. Kitchen, *Food Chem.*, **314**, 126180 (2020); https://doi.org/10.1016/j.foodchem.2020.126180
7. W.R. Jaffé, *Sugar Tech*, **14**, 87 (2012); https://doi.org/10.1007/s12355-012-0145-1
8. C. Srinivasulu, M. Ramgopal, G. Ramanjaneyulu, C.M. Anuradha and C. Suresh Kumar, *Biomed. Pharmacother.*, **108**, 547 (2018); https://doi.org/10.1016/j.biopha.2018.09.069
9. B.C. Sahoo, S. Sahoo, S. Nayak and B. Kar, *Plant Sci. Today*, **9**, 81 (2021); https://doi.org/10.14719/pst.1102

10. F. Ayustaningwarno, G. Anjani, A.M. Ayu and V. Fogliano, *Front. Nutr.*, **11**, 1364836 (2024); https://doi.org/10.3389/fnut.2024.1364836
11. B. Ahmad, M. U. Rehman, I. Amin, A. Arif, S. Rasool, S. A. Bhat, I. Afzal, I. Hussain, S. Bilal and M.R. Mir, *Scientific World J.*, **2015**, 816364 (2015); https://doi.org/10.1155/2015/816364
12. S. Shashikala B.V, S. Ampeti, M. Srivastava, S.R. Sali and RB. Sheikh, *medtigo J. Pharmacol.*, **1**, e3061113 (2024); https://doi.org/10.63096/medtigo3061113
13. R. Gupta, P.K. Singh, R. Singh and R.L. Singh, *In. J. Scient. Innov. Res.*, **4**, 1 (2016).
14. M. Chieppa, S. De Santis and G. Verna, *Inflamm. Bowel Dis.*, **31**, 1158 (2025); https://doi.org/10.1093/ibd/izaf006
15. R. Khanna, A.S. Wilson, J.C. Gregor, K.L. Prowse and W. Afif, *Gastroenterology*, **161**, 2059 (2021); https://doi.org/10.1053/j.gastro.2021.09.021
16. A.N. Ananthakrishnan, *Nat. Rev. Gastroenterol. Hepatol.*, **12**, 205 (2015); https://doi.org/10.1038/nrgastro.2015.34
17. S.M. Wilhelm and B.L. Love, *Clin. Pharm.*, **9**, 3 (2017); https://doi.org/10. 1211/PJ.2017.20202316
18. J. Jang and S. Jeong, *Biochip J.*, **17**, 403 (2023); https://doi.org/10.1007/s13206-023-00118-y
19. M.J. Frisch, G.W. Trucks, H.B. Schlegel, G.E. Scuseria, M.A. Robb, J.R. Cheeseman, G. Scalmani, V. Barone, G.A. Petersson, H. Nakatsuji, X. Li, M. Caricato, A. V. Marenich, J. Bloino, B. G. Janesko, R. Gomperts, B. Mennucci, H.P. Hratchian, A.F. Izmaylov, J.L. Sonnenberg, J.V. Ortiz, D. Williams-Young, F. Ding, F. Lipparini, F. Egidi, J. Goings, B. Peng, A. Petrone, T. Henderson, D. Ranasinghe, V.G. Zakrzewski, J. Gao, N. Rega, G. Zheng, W. Liang, M. Hada, M. Ehara, K. Toyota, R. Fukuda, J. Hasegawa, M. Ishida, T. Nakajima, Y. Honda, O. Kitao, H. Nakai, T. Vreven, K. Throssell, J. A. Montgomery, Jr., J.E. Peralta, F. Ogliaro, M.J. Bearpark, J.J. Heyd, E.N. Brothers, K.N. Kudin, V.N. Staroverov, T.A. Keith, R. Kobayashi, J. Normand, K. Raghavachari, A.P. Rendell, J.C. Burant, S.S. Iyengar, J. Tomasi, M. Cossi, J.M. Millam, M. Klene, C. Adamo, R. Cammi, J.W. Ochterski, R.L. Martin, K. Morokuma, O. Farkas, J.B. Foresman and D.J. Fox, Gaussian 16, Revision A. 03, Gaussian Inc., Wallingford, CT (2016);
20. R. Dennington, T. Keith and J. Millam, Semichem Inc., Shawnee Mission KS, GaussView, Version 5 (2009).
21. A.D. Becke, *J. Chem. Phys.*, **98**, 5648 (1993); https://doi.org/10.1063/1.464913
22. M.H. Jamróz, *Spectrochim. Acta A Mol. Biomol. Spectrosc.*, **114**, 220 (2013); https://doi.org/10.1016/j.saa.2013.05.096
23. N.M. O'boyle, A.L. Tenderholt and K.M. Langner, *J. Comput. Chem.*, **29**, 839 (2008); https://doi.org/10.1002/jcc.20823
24. T. Lu and F. Chen, *J. Comput. Chem.*, **33**, 580 (2012); https://doi.org/10.1002/jcc.22885
25. W. Humphrey, A. Dalke and K. Schulten, *J. Mol. Graph.*, **14**, (1996); https://doi.org/10.1016/0263-7855(96)00018-5
26. A. Daina, O. Michielin and V. Zoete, *Sci. Rep.*, **7**, 42717 (2017); https://doi.org/10.1038/srep42717
27. R.A. Laskowski, M.W. MacArthur, D.S. Moss and J.M. Thornton, *J. Appl. Cryst.*, **26**, 283 (1993); https://doi.org/10.1107/S0021889892009944
28. R. Huey, G.M. Morris and S. Forli, Using AutoDock 4 and AutoDock vina with AutoDockTools: A Tutorial, The Scripps Research Institute, California, USA (2012).
29. R.O. Jones and O. Gunnarsson, *Rev. Mod. Phys.*, **61**, 689 (1989); https://doi.org/10.1103/RevModPhys.61.689
30. F.H. Allen, O. Kennard, D.G. Watson, L. Brammer, A.G. Orpen and R. Taylor, *J. Chem. Soc., Perkin Trans. II*, **2**, S1 (1987); https://doi.org/10.1039/p298700000s1
31. J. Laane, *J. Phys. Chem. A*, **104**, 7715 (2000); https://doi.org/10.1021/jp0009002
32. G. Fogarasi, J.E. Boggs and P. Pulay, *Mol. Phys.*, **50**, 139 (1983); https://doi.org/10.1080/00268978300102231
33. M.P. Andersson and P. Uvdal, *J. Phys. Chem. A*, **109**, 2937 (2005); https://doi.org/10.1021/jp045733a
34. K. Nakamoto, Infrared and Raman Spectra of Inorganic and Coordination Compounds, Part B: Applications in Coordination, Organometallic and Bioinorganic Chemistry, John Wiley & Sons, (2009).
35. R.M. Silverstein and G.C. Bassler, *J. Chem. Educ.*, **39**, 546 (1962); https://doi.org/10.1021/ed039p546
36. K. Garima, A. Fatima, K. Pooja, S. Savita, M. Sharma, M. Kumar, S. Muthu, N. Siddiqui, and S. Javed, *Polycycl. Arom. Compds.*, **43**, 7828 (2022); https://doi.org/10.1080/10406638.2022.2140681
37. B.C. Smith, Fundamentals of Fourier Transform Infrared Spectroscopy, CRC Press (1996).
38. P. Ramesh, M. Lydia Caroline, S. Muthu, B. Narayana, M. Raja and S. Aayisha, *J. Mol. Struct.*, **1200**, 127123 (2020); https://doi.org/10.1016/j.molstruc.2019.127123
39. K. Hemachandran, P. Anbusrinivasan, S. Ramalingam, R. Aarthi and C.K. Nithya, *Heliyon*, **5**, e02788 (2019); https://doi.org/10.1016/j.heliyon.2019.e02788
40. B.F. Rizwana, J.C. Prasana and S. Muthu, *Int. J. Mater. Sci.*, **12**, 196 (2017).
41. V.A. Pathade, R.H. Waghchaure, B.S. Jagdale, T.B. Pawar and S.S. Pathade, *Int. J. Adv. Sci. Res.*, **11 (Suppl 2)**, 64 (2020);
42. M. Miar, A. Shiroudi, K. Pourshamsian, A.R. Oliaey and F. Hatamjafari, *J. Chem. Res.*, **45**, 147 (2021); https://doi.org/10.1177/1747519820932091
43. J.D. Magdaline and T. Chithambarathanu, *IOSR J. Appl. Chem.*, **8**, (2015); https://doi.org/10.9790/5736-08510614
44. A. Dreuw and M. Head-Gordon, *Chem. Rev.*, **105**, 4009 (2005); https://doi.org/10.1021/cr0505627
45. B. Silvi and A. Savin, *Nature*, **371**, 683 (1994); https://doi.org/10.1038/371683a0
46. J.N. Israelachvili, *Contemp. Phys.*, **15**, 159 (1974); https://doi.org/10.1080/00107517408210785
47. B. Bakchi, A.D. Krishna, E. Sreecharan, V.B.J. Ganesh, M. Niharika, S. Maharshi, S.B. Puttagunta, D.K. Sigalapalli, R.R. Bhandare and A.B. Shaik, *J. Mol. Struct.*, **1259**, 132712 (2022); https://doi.org/10.1016/j.molstruc.2022.132712
48. A. Daina and V. Zoete, *ChemMedChem*, **11**, 1117 (2016); https://doi.org/10.1002/cmdc.201600182
49. R. Shimazu, M. Anada, A. Miyaguchi, Y. Nomi and H. Matsumoto, *J. Agric. Food Chem.*, **69**, 11676 (2021); https://doi.org/10.1021/acs.jafc.1c02898